Dialysis technique. The materials of the dialysis probe were the same as those used in our previous dialysis experiments (1, 2). Briefly, each end of the dialysis fiber (0.31 mm OD, and 0.20 mm ID; PAN-1200 50,000 mol wt cutoff, Asahi Chemical) was inserted into the polyethylene tube (25-cm length, 0.5 mm OD, and 0.2 mm ID; SP-8) and glued. The length of the dialysis fiber exposed was 3 mm.

The left adrenal gland was gently lifted, and the dialysis probe was implanted in the medulla of the left adrenal gland along the long axis by using a fine guiding needle. The dialysis probe was perfused with Ringer solution containing a cholinesterase inhibitor, neostigmine (10 μM), at a speed of 10 μl/min using a microinjection pump (CMA/100, Carnegie Medicin). Ringer solution with no buffer consisted of (in mM) 147.0 NaCl, 4.0 KCl, and 2.25 $CaCl_2$. One sampling period was 2 min (1 sample volume = 20 μl). We started the protocols followed by a stabilization period of 3–4 h and sampled dialysate taking the dead space volume into account.

Dialysate ACh, norepinephrine (NE), and epinephrine (Epi) concentrations were measured as indexes of ACh and catecholamine releases in the adrenal medulla. Half of the dialysate sample was used for the measurement of ACh, and the remaining half for the measurement of NE and Epi. ACh and catecholamine assays were separately conducted using each high-performance liquid chromatography with electrochemical detection as previously described (3, 4).

Experimental design. The experiment was performed based on the previous experiment showing that dialysate ACh and catecholamine responses were reproducible on repetition of stimulation (2). The left splanchnic nerves were electrically stimulated for 2 min at 30-min intervals. Three dialysate samples were continuously collected per electrical stimulation: one before, one during, and one after stimulation. Stimulations at two different frequencies (2 and 4 Hz) were performed before and after intravenous administration of Ca^{2+} channel antagonists.

We tested three types of Ca^{2+} channel antagonists (25): the N-type Ca^{2+} channel antagonist ω-conotoxin GVIA, the P/Q-type Ca^{2+} channel antagonist ω-conotoxin MVIIC, and the L-type Ca^{2+} channel antagonist nifedipine. We determined the first doses of Ca^{2+} channel antagonists based on the dose used in the earlier experiments (7, 14, 26, 29, 37) and tested ω-conotoxin GVIA (10 μg/kg) in six rats, ω-conotoxin MVIIC (50 μg/kg) in six rats, and nifedipine (300 μg/kg) in six rats. Second, we tested a fivefold higher dose of ω-conotoxin GVIA (50 μg/kg) in six rats, a combination of fivefold higher doses of ω-conotoxin GVIA (50 μg/kg) and MVIIC (250 μg/kg) in six rats, and a threefold higher dose of nifedipine (900 μg/kg) in six rats. We did not test a higher dose of ω-conotoxin MVIIC singly because a high dose of ω-conotoxin MVIIC loses its selectivity for P/Q-type and inhibits N-type Ca^{2+} channels (18).

Nifedipine was administered twice before 2- and 4-Hz stimulation, but ω-conotoxin GVIA and MVIIC were administered once before 2-Hz stimulation because the ω-conotoxin family has long-lasting blocking actions (8, 18, 36). We assessed the responses to nerve stimulation 30, 20, and 10 min after administration of ω-conotoxin GVIA, ω-conotoxin MVIIC, and nifedipine, respectively, when heart rate and arterial pressure had already been stabilized.

At the end of the experiment the rats were killed with pentobarbital sodium, and the implant sites were examined. The dialysis probes were confirmed to have been implanted in the adrenal medulla, and no bleeding or necrosis was found macroscopically.

Drugs. Drugs were mixed fresh for each experiment. Neostigmine methylsulfate (Shionogi), ω-conotoxin GVIA (Peptide Institute), and ω-conotoxin MVIIC (Peptide Institute) were dissolved and diluted in Ringer solution. Nifedipine (Sigma Chemical) was dissolved in ethanol and diluted in Ringer solution.

Statistical methods. To examine the effects of nerve stimulation and Ca^{2+} channel antagonists, we analyzed heart rate and mean arterial pressure and dialysate ACh, NE, and Epi responses by using one-way ANOVA with repeated measures. When statistical significance was detected, the Newman-Keuls test was applied (35). Statistical significance was defined as $P < 0.05$. Values are presented as means ± SE.

RESULTS

Effects of Ca^{2+} channel antagonists on heart rate and mean arterial pressure. ω-Conotoxin GVIA (10 μg/kg) decreased heart rate from 418 ± 9 to 328 ± 13 beats/min ($P < 0.05$) and mean arterial pressure from 115 ± 2 to 74 ± 2 mmHg ($P < 0.05$). ω-Conotoxin GVIA (50 μg/kg) did not further decrease heart rate and mean arterial pressure. ω-Conotoxin MVIIC decreased heart rate from 408 ± 3 to 390 ± 5 beats/min ($P < 0.05$) but did not change mean arterial pressure. Combined ω-conotoxin GVIA and MVIIC decreased heart rate from 415 ± 10 to 327 ± 4 beats/min ($P < 0.05$) and mean arterial pressure from 124 ± 2 to 57 ± 2 mmHg ($P < 0.05$). Nifedipine (300 μg/kg) decreased mean arterial pressure from 113 ± 4 to 86 ± 4 mmHg ($P < 0.05$) but did not change heart rate. Nifedipine (900 μg/kg) decreased mean arterial pressure from 124 ± 3 to 73 ± 2 mmHg ($P < 0.05$).

Effects of Ca^{2+} channel antagonists on ACh and catecholamine releases. ACh could not be detected in dialysate before or after stimulation. Thus we expressed dialysate ACh concentration during stimulation as an index of ACh release induced by stimulation. In contrast, substantial amounts of NE and Epi were observed in dialysate before stimulation. Intravenous administration of Ca^{2+} channel antagonists did not affect these basal NE and Epi releases (Table 1). Dialysate NE and Epi concentrations increased by nerve stimulation and rapidly declined after the stimulation. Thus we subtracted the dialysate NE and Epi contents before stimulation from those during stimulation and expressed these values as indexes of NE and Epi releases induced by stimulation.

Effects of ω-conotoxin GVIA. ω-Conotoxin GVIA (10 μg/kg) significantly inhibited ACh release at 2 Hz from 6.2 ± 0.9 to 3.6 ± 0.5 nM, ACh release at 4 Hz from 12.2 ± 1.7 to 7.9 ± 1.2 nM, NE release at 4 Hz from 34 ± 6 to 17 ± 3 nM, Epi release at 2 Hz from 81 ± 13 to 42 ± 3 nM, and Epi release at 4 Hz from 180 ± 21 to 94 ± 7 nM. However, inhibition of NE release at 2 Hz was not statistically significant (Fig. 1*A*). A fivefold higher dose of ω-conotoxin GVIA (50 μg/kg) did not

Table 1. *Basal dialysate NE and Epi concentrations before and after administration of Ca^{2+} channel antagonists*

	NE, nM	Epi, nM
ω-Conotoxin GVIA (10 and 50 μg/kg) (n = 12)		
Before administration	4.9±0.9	20.6±2.9
After administration	3.8±0.6	21.0±2.6
ω-Conotoxin MVIIC (50 μg/kg) (n = 6)		
Before administration	4.1±1.0	20.2±2.6
After administration	4.6±0.9	24.0±3.5
ω-Conotoxin GVIA (50 μg/kg) + MVIIC (250 μg/kg) (n = 6)		
Before administration	4.4±1.3	17.5±3.8
After administration	3.1±0.7	20.8±4.4
Nifedipine (100 and 300 μg/kg) (n = 12)		
Before administration	4.0±0.6	17.4±2.2
After administration	3.3±0.9	17.7±2.9

Values are means ± SE; *n*, no. of rats. NE, norepinephrine; Epi, epinephrine.

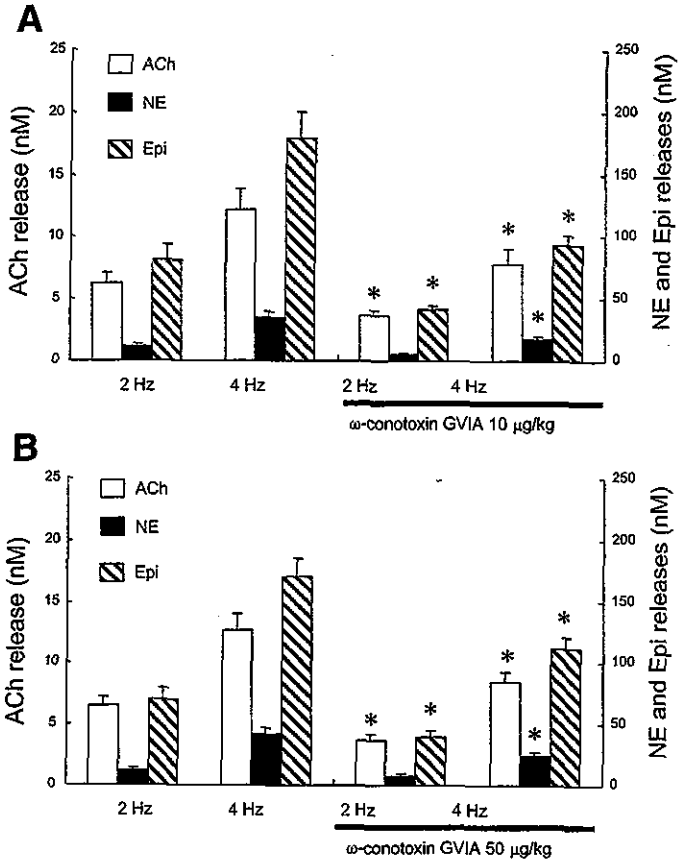

Fig. 1. Effects of ω-conotoxin GVIA on ACh, norepinephrine (NE), and epinephrine (Epi) releases. ω-Conotoxin GVIA (10 μg/kg) inhibited ACh release at 2 and 4 Hz, NE release at 4 Hz, and Epi release at 2 and 4 Hz (*A*). A 5-fold higher dose of ω-conotoxin GVIA (50 μg/kg) did not further inhibit these releases (*B*). Values are means ± SE from 6 rats. $*P < 0.05$ vs. ACh, NE, or Epi release at same frequency before administration.

further inhibit release. ω-Conotoxin GVIA (50 μg/kg) significantly inhibited ACh release at 2 Hz from 6.5 ± 0.7 to 3.7 ± 0.5 nM, ACh release at 4 Hz from 12.6 ± 1.4 to 8.5 ± 0.8 nM, NE release at 4 Hz from 41 ± 6 to 24 ± 4 nM, Epi release at 2 Hz from 70 ± 10 to 40 ± 6 nM, and Epi release at 4 Hz from 170 ± 15 to 112 ± 10 nM (Fig. 1*B*).

Effects of ω-conotoxin MVIIC. ω-Conotoxin MVIIC (50 μg/kg) significantly inhibited ACh release at 4 Hz from 11.7 ± 2.5 to 8.5 ± 2.1 nM and Epi release at 4 Hz from 170 ± 38 to 129 ± 35 nM. Inhibitions of ACh and Epi releases at 2 Hz and NE release at either frequency were not statistically significant (Fig. 2).

Effects of combined ω-conotoxin GVIA and MVIIC. Combined ω-conotoxin GVIA (50 μg/kg) and MVIIC (250 μg/kg) significantly inhibited ACh release at 2 Hz from 6.7 ± 0.6 to 1.9 ± 0.3 nM, ACh release at 4 Hz from 12.1 ± 1.3 to 3.8 ± 0.6 nM, NE release at 2 Hz from 11.1 ± 1.1 to 1.2 ± 0.3 nM, NE release at 4 Hz from 36 ± 5 to 8 ± 2 nM, Epi release at 2 Hz from 88 ± 9 to 13 ± 3 nM, and Epi release at 4 Hz from 187 ± 20 to 49 ± 9 nM (Fig. 3).

Effects of nifedipine. Nifedipine (300 μg/kg) did not change ACh release at either frequency but significantly inhibited Epi release at 4 Hz from 172 ± 31 to 135 ± 23 nM. Inhibitions of Epi release at 2 Hz and NE release at either frequency were not statistically significant (Fig. 4*A*). A threefold higher dose of

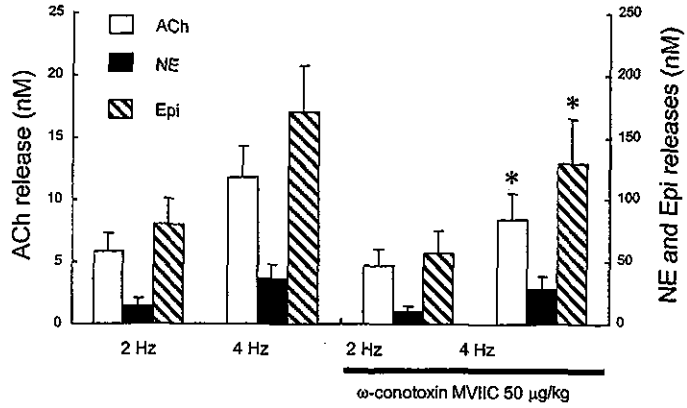

Fig. 2. Effects of ω-conotoxin MVIIC on ACh, NE, and Epi releases. ω-Conotoxin MVIIC (50 μg/kg) inhibited ACh and Epi releases at 4 Hz. Values are means ± SE from 6 rats. $*P < 0.05$ vs. ACh, NE, or Epi release at same frequency before administration.

nifedipine (900 μg/kg) did not change ACh release but significantly inhibited Epi release at 4 Hz from 188 ± 24 to 128 ± 15 nM and NE release at 4 Hz from 33 ± 5 to 24 ± 4 nM. Inhibitions of NE and Epi releases at 2 Hz were not statistically significant (Fig. 4*B*).

DISCUSSION

Effects of Ca^{2+} channel antagonists on ACh release from splanchnic nerve endings. In the present study, ω-conotoxin GVIA (10 μg/kg) inhibited ACh release at both 2 and 4 Hz by approximately 35–40%. A fivefold higher dose of ω-conotoxin GVIA (50 μg/kg) did not further inhibit ACh release. ω-Conotoxin MVIIC (50 μg/kg) inhibited ACh release at 4 Hz by ~30%. Combined ω-conotoxin GVIA (50 μg/kg) and MVIIC (250 μg/kg) inhibited ACh release at both 2 and 4 Hz by ~70%. N- and P/Q-type Ca^{2+} channels could be present on the splanchnic nerve endings and be involved in ACh release. P/Q-type Ca^{2+} channels may play a role in ACh release at a high frequency of stimulation. ACh release response was resistant to nifedipine (300 and 900 μg/kg) at both 2 and 4 Hz. L-type Ca^{2+} channels could not be present on splanchnic nerve

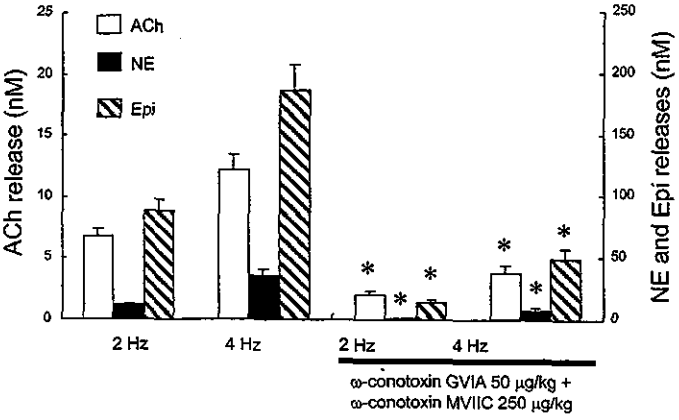

Fig. 3. Effects of combined ω-conotoxin GVIA and MVIIC on ACh, NE, and Epi releases. Combined ω-conotoxin GVIA (50 μg/kg) and MVIIC (250 μg/kg) inhibited ACh, NE, and Epi releases at 2 and 4 Hz. Values are means ± SE from 6 rats. $*P < 0.05$ vs. ACh, NE, or Epi release at same frequency before administration.

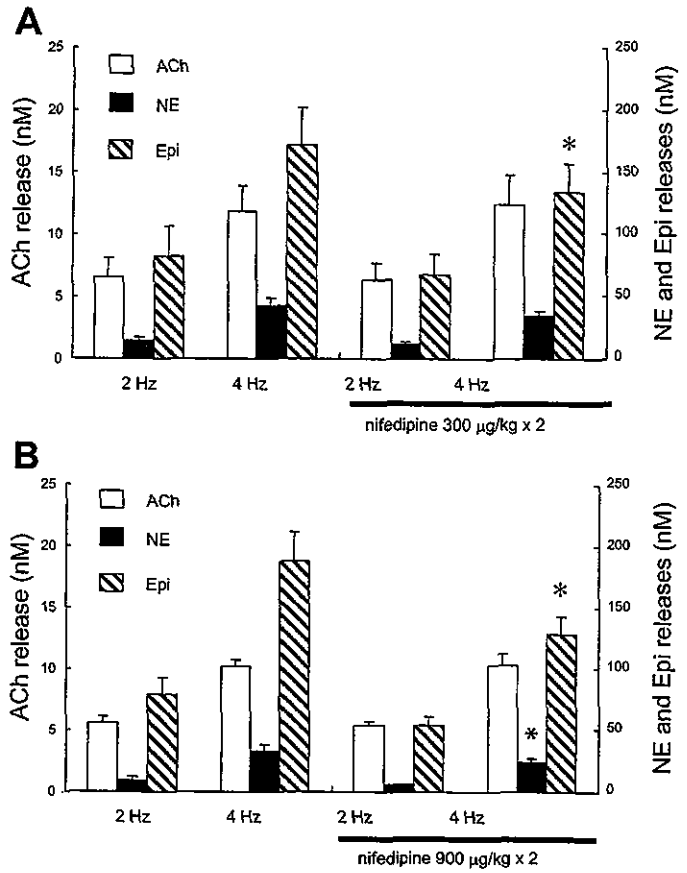

Fig. 4. Effects of nifedipine on ACh, NE, and Epi releases. Nifedipine (300 μg/kg) did not change ACh release at either frequency but inhibited Epi release at 4 Hz (*A*). Nifedipine (900 μg/kg) did not change ACh release at either frequency but inhibited NE and Epi releases at 4 Hz (*B*). Values are means ± SE from 6 rats. $*P < 0.05$ vs. ACh, NE, or Epi release at same frequency before administration.

endings or not play a major role in ACh release. This is the first direct study to demonstrate the type of Ca^{2+} channels controlling ACh release from splanchnic nerve endings.

In isolated rat adrenal glands, catecholamine release induced by field stimulation is sensitive to P/Q-type Ca^{2+} channel antagonist, whereas that induced by exogenous ACh is insensitive (27). This indirect study suggested the involvement of P/Q-type Ca^{2+} channels in ACh release but failed to show the involvement of N-type Ca^{2+} channels. In isolated bovine adrenal glands, a direct measurement study showed that a reduction of the extracellular Ca^{2+} concentration inhibits ^{3}H-labeled ACh release induced by field stimulation, but N- and L-type Ca^{2+} channel antagonists do not (28). Thus our findings are in part consistent with these direct and indirect studies but inconsistent as to the involvement of N-type Ca^{2+} channels.

This discrepancy might be ascribed to the experimental method. The contribution of Ca^{2+} channels may vary with the type of method used to evoke ACh release. In these studies, ACh release was evoked by electrical field stimulation of isolated adrenal glands, which is known to induce ACh release but not direct depolarization of chromaffin cells (34). In the present study, ACh release was evoked in the in vivo state by electrical stimulation of splanchnic nerves. The type of Ca^{2+} channels involved in ACh release may vary with the frequency, amplitude, or time period of stimulation. Actually, in the present study, we observed the involvement of P/Q-type Ca^{2+} channels at only high-frequency stimulation, while it has been reported in perfused rat adrenal glands that N-type Ca^{2+} channels are involved in the maintenance of catecholamine release in response to long splanchnic nerve stimulation (31). The time period of 2 min in the present study seems to be longer than those in earlier studies but could be within the physiological range. Moreover, the blocking action of ω-conotoxin GVIA is time dependent as well as dose dependent and irreversible (8, 11, 32, 36). The maximum functional effect of ω-conotoxin GVIA has been observed to be at least 15 min after administration. We evaluated the effect of ω-conotoxin GVIA 30 min after intravenous administration, when heart rate and mean arterial pressure had already been stabilized. The evaluation early after administration might lead to underestimation of the inhibitory effects of ω-conotoxin GVIA.

There are many similarities between synaptic transmission from splanchnic nerves to chromaffin cells and sympathetic ganglionic transmission (17). In isolated guinea pig paravertebral ganglia, an electrophysiological study has shown that both N- and P-type Ca^{2+} channel antagonists reduce cholinergic synaptic conductance, whereas L-type Ca^{2+} channel antagonist does not (19). In isolated rat superior cervical ganglia, both N- and P-type Ca^{2+} channel antagonists inhibit the rise in Ca^{2+} concentration in the terminal boutons (22). Moreover, in isolated rat superior cervical ganglia, ^{3}H-labeled ACh release induced by high K^+ is inhibited by both N- and P-type Ca^{2+} channel antagonists but unaffected by L-type Ca^{2+} channel antagonist (15). Our findings are similar to these findings obtained from isolated sympathetic preganglionic nerves.

The inhibition by ω-conotoxin GVIA (50 μg/kg) was almost the same as that by ω-conotoxin GVIA (10 μg/kg). Moreover, the inhibition by combined ω-conotoxin GVIA (50 μg/kg) and MVIIC (250 μg/kg) was almost algebraically the sum of the individual inhibition by ω-conotoxin GVIA (10 μg/kg) and MVIIC (50 μg/kg). These results suggest that fivefold higher doses of ω-conotoxin GVIA and MVIIC are sufficient to cause inhibition of Ca^{2+} channels. However, ~30% of ACh release was resistant to combined ω-conotoxin GVIA (50 μg/kg) and MVIIC (250 μg/kg). Other types of Ca^{2+} channels except for N- and P/Q-types may be involved in ACh release from splanchnic nerve endings. Further examination could be needed.

Effects of Ca^{2+} channel antagonists on catecholamine release from chromaffin cells. In the present study, nifedipine (300 μg/kg) did not change ACh release at 2 and 4 Hz but inhibited Epi release at 4 Hz by ~20%. A threefold higher dose of nifedipine (900 μg/kg) did not change ACh release at 2 and 4 Hz but inhibited NE and Epi releases at 4 Hz by ~30%. Adrenal chromaffin cells are divided into two populations: NE- and Epi-storing cells (10). L-type Ca^{2+} channels could be present on the surface of both NE- and Epi-storing cells and play a role in NE and Epi releases.

Approximately 70% of catecholamine release was resistant to nifedipine (900 μg/kg). This result suggests that other types of Ca^{2+} channels except for L-type are present on chromaffin cells and involved in NE and Epi releases, although we cannot exclude the possibility of incomplete inhibition of L-type Ca^{2+} channels. Species differences in the types of Ca^{2+} channels controlling Ca^{2+} influx and catecholamine release have been

shown with rat, cat, and bovine chromaffin cells (5, 6, 13, 24). In patch-clamp studies of isolated rat chromaffin cells, Ca^{2+} inward current elicited by depolarization is sensitive to both L- and N-type Ca^{2+} channel antagonists (16, 21). The study measuring Ba^{2+} current by patch-clamp technique has shown the existence of L-, N-, and P/Q-type Ca^{2+} channels on rat chromaffin cells and the following distribution of Ca^{2+} channels in decreasing order: L-type > N-type > P/Q-type (13). In the present study, ω-conotoxin GVIA (10 and 50 μg/kg) inhibited NE release at 4 Hz and Epi release at 2 and 4 Hz by approximately 45–50%. ω-Conotoxin MVIIC (50 μg/kg) inhibited Epi release at 4 Hz by ~30%. Combined ω-conotoxin GVIA (50 μg/kg) and MVIIC (250 μg/kg) inhibited NE and Epi releases at 2 and 4 Hz by approximately 75–85%. However, these Ca^{2+} channel antagonists simultaneously inhibited ACh release to almost the same extent. It is difficult to determine how much Ca^{2+} antagonists are acting on chromaffin cells when Ca^{2+} channel antagonists inhibit ACh release. Thus, although much of these inhibitions of catecholamine release may be considered to be consequences of the inhibition of ACh release, we cannot exclude the possibility that N- or P/Q-type Ca^{2+} channels may be involved in the in vivo catecholamine release on chromaffin cells.

The inhibition of NE release at 2 Hz by ω-conotoxin GVIA (10 and 50 μg/kg) and the inhibition of NE release at 4 Hz by ω-conotoxin MVIIC (50 μg/kg) were not statistically significant despite significant inhibitions of ACh and Epi releases. In the same preparation, we have shown that cholinergic antagonists almost inhibited NE and Epi releases induced by nerve stimulation (1, 2). However, the correlation between ACh and NE releases was poorer than that between ACh and Epi releases when stimulation frequency was raised stepwise (2). Insignificant inhibitions of NE release may be ascribed to this poor correlation.

In the present study, Ca^{2+} channel antagonists did not affect basal dialysate NE and Epi levels. In our previous study of the same preparation, these basal levels were not affected by neostigmine, hexamethonium, or atropine (1). We then concluded that these basal dialysate NE and Epi levels reflect noncholinergic catecholamine release. N-, P/Q-, and L-type Ca^{2+} channels may not play a major role in basal noncholinergic catecholamine release from adrenal medulla.

Methodological considerations. We administered neostigmine locally to adrenal medulla through a dialysis probe. Cholinesterase inhibitor was necessary to monitor endogenous ACh even during splanchnic nerve stimulation because released ACh is rapidly degraded by acetylcholinesterase before reaching the dialysis fiber. In the same preparation, local administration of neostigmine enhanced the dialysate catecholamine response to nerve stimulation by approximately threefold, but dialysate ACh and catecholamine responses are correlated with the stimulation frequency of splanchnic nerves in the presence of neostigmine (2). Thus dialysate ACh and catecholamine responses are likely to be correlated with the amount of Ca^{2+} influx from voltage-dependent Ca^{2+} channels even in the presence of neostigmine.

Intravenous administration of Ca^{2+} channel antagonists induced changes in heart rate or mean arterial pressure. These changes might affect ACh and catecholamine releases through a baroreflex mechanism. Moreover, these hemodynamic changes might decrease the spillover of ACh or catecholamine from adrenal medulla and affect the dialysate ACh or catecholamine concentrations (20). In our preparation, however, splanchnic nerves had been transected before control sampling, and basal dialysate catecholamine concentrations did not change before or after administration. Thus effects of these hemodynamic changes could be negligible when we considered the effects of Ca^{2+} channel antagonists on nerve stimulation-induced dialysate responses.

In conclusion, we applied dialysis technique to the adrenal medulla of anesthetized rats and investigated the effects of Ca^{2+} channel antagonists on ACh and catecholamine releases induced by electrical stimulation of splanchnic nerves. Both N- and P/Q-type Ca^{2+} channels control ACh release on preganglionic splanchnic nerve endings while L-type Ca^{2+} channels do not. L-type Ca^{2+} channels are involved in norepinephrine and epinephrine releases on chromaffin cells.

GRANTS

This study was supported by the Program for Promotion of Fundamental Studies in Health Science of the Organization for Pharmaceutical Safety and Research (of Japan); by a Health Sciences Research Grant for Advanced Medical Technology from the Ministry of Health and Welfare of Japan; by a Ground-Based Research Grant for the Space Utilization promoted by the National Space Development Agency of Japan and Japan Space Forum; and by grants-in-aid for scientific research from the Ministry of Education, Science.

REFERENCES

1. **Akiyama T, Yamazaki T, Mori H, and Sunagawa K.** Inhibition of cholinesterase elicits muscarinic receptor-mediated synaptic transmission in the rat adrenal medulla. *Auton Neurosci* 107: 65–73, 2003.
2. **Akiyama T, Yamazaki T, Mori H, and Sunagawa K.** Simultaneous monitoring of acetylcholine and catecholamine release in the in vivo rat adrenal medulla. *Neurochem Int* 44: 497–503, 2004.
3. **Akiyama T, Yamazaki T, and Ninomiya I.** In vivo detection of endogenous acetylcholine release in cat ventricles. *Am J Physiol Heart Circ Physiol* 266: H854–H860, 1994.
4. **Akiyama T, Yamazaki T, and Ninomiya I.** In vivo monitoring of myocardial interstitial norepinephrine by dialysis technique. *Am J Physiol Heart Circ Physiol* 261: H1643–H1647, 1991.
5. **Albillos A, Artalejo AR, López MG, Gandía L, García AG, and Carbone E.** Calcium channel subtypes in cat chromaffin cells. *J Physiol* 477: 197–213, 1994.
6. **Artalejo CR, Perlman RL, and Fox AP.** ω-Conotoxin GVIA blocks a Ca^{2+} current in bovine chromaffin cells that is not of the "classic" N type. *Neuron* 8: 85–95, 1992.
7. **Buckingham RE.** Studies on the anti-vasoconstrictor activity of BRL 34915 in spontaneously hypertensive rats; a comparison with nifedipine. *Br J Pharmacol* 93: 541–552, 1988.
8. **Clasbrummel B, Osswald H, and Illes P.** Inhibition of noradrenaline release by ω-conotoxin GVIA in the rat tail artery. *Br J Pharmacol* 96: 101–110, 1989.
9. **Coupland RE.** *The Natural History of the Chromaffin Cell.* London: Longmans, 1965.
10. **Coupland RE.** Ultrastructural features of the mammalian adrenal medulla. In: *Ultrastructure of Endocrine Cells and Tissues*, edited by Motta PM. Boston, MA: Nijhoff, 1984, p. 168–179.
11. **De Luca A, Li CG, Rand MJ, Reid JJ, Thaina P, and Wong-Dusting HK.** Effects of ω-conotoxin GVIA on autonomic neuroeffector transmission in various tissues. *Br J Pharmacol* 101: 437–447, 1990.
12. **Dunlap K, Luebke JI, and Turner TJ.** Exocytotic Ca^{2+} channels in mammalian central neurons. *Trends Neurosci* 18: 89–98, 1995.
13. **Gandía L, Borges R, Albillos A, and García AG.** Multiple calcium channel subtypes in isolated rat chromaffin cells. *Pflügers Arch* 430: 55–63, 1995.
14. **Gaspo R, Yamaguchi N, and de Champlain J.** Nifedipine inhibits adrenal but not circulating catecholamine response to nicotinic stimulation in dogs. *Am J Physiol Regul Integr Comp Physiol* 267: R1545–R1551, 1994.
15. **Gonzalez Burgos GR, Biali FI, Cherksey BD, Sugimori M, Llinas RR, and Uchitel OD.** Different calcium channels mediate transmitter release

evoked by transient or sustained depolarization at mammalian sympathetic ganglia. *Neuroscience* 64: 117–123, 1995.

16. **Hollins B and Ikeda SR.** Inward currents underlying action potentials in rat adrenal chromaffin cells. *J Neurophysiol* 76: 1195–1211, 1996.
17. **Holman ME, Coleman HA, Tonta MA, and Parkington HC.** Synaptic transmission from splanchnic nerves to the adrenal medulla of guinea-pigs. *J Physiol* 478: 115–124, 1994.
18. **Hillyard DR, Monje VD, Mintz IM, Bean BP, Nadasdi L, Ramachandran J, Miljanich G, Azimi-Zoonooz A, McIntosh JM, Cruz LJ, Imperial JS, and Olivera BM.** A new Conus peptide ligand for mammalian presynaptic Ca^{2+} channels. *Neuron* 9: 69–77, 1992.
19. **Ireland DR, Davies PJ, and McLachlan EM.** Calcium channel subtypes differ at two types of cholinergic synapse in lumbar sympathetic neurones of guinea-pigs. *J Physiol* 514: 59–69, 1999.
20. **Kawada T, Yamazaki T, Akiyama T, Shishido T, Inagaki M, Uemura K, Miyamoto T, Sugimachi M, Takaki H, and Sunagawa K.** In vivo assessment of acetylcholine-releasing function at cardiac vagal nerve terminals. *Am J Physiol Heart Circ Physiol* 281: H139–H145, 2001.
21. **Kim SJ, Lim W, and Kim J.** Contribution of L- and N-type calcium currents to exocytosis in rat adrenal medullary chromaffin cells. *Brain Res* 675: 289–296, 1995.
22. **Lin YQ, Brain KL, and Bennett MR.** Calcium in sympathetic boutons of rat superior cervical ganglion during facilitation, augmentation and potentiation. *J Auton Nerv Syst* 73: 26–37, 1998.
23. **Lomax RB, Michelrna P, Núñez L, García-Sancho J, García AG, and Montiel C.** Different contributions of L- and Q-type Ca^{2+} channels to Ca^{2+} signals and secretion in chromaffin cell subtypes. *Am J Physiol Cell Physiol* 272: C476–C484, 1997.
24. **López MG, Albillos A, de la Fuente MT, Borges R, Gandía L, Carbone E, García AG, and Artalejo AR.** Localized L-type calcium channels control exocytosis in cat chromaffin cells. *Pflügers Arch* 427: 348–354, 1994.
25. **Meir A, Ginsburg S, Butkevich A, Kachalsky SG, Kaiserman I, Ahdut R, Demirgoren S, and Rahamimoff R.** Ion channels in presynaptic nerve terminals and control of transmitter release. *Physiol Rev* 79: 1019–1088, 1999.
26. **Morimoto H, Matsuda A, Ohori M, and Fujii T.** Effects of ω-conotoxin GVIA on the activation of capsaicin-sensitive afferent sensory nerves in guinea pig airway tissues. *Jpn J Pharmacol* 71: 161–166, 1996.
27. **Nagayama T, Matsumoto T, Kuwakubo F, Fukushima Y, Yoshida M, Suzuki-Kusaba M, Hisa H, Kimura T, and Satoh S.** Role of calcium channels in catecholamine secretion in the rat adrenal gland. *J Physiol* 520: 503–512, 1999.
28. **O'Farrell M, Ziogas J, and Marley PD.** Effects of N- and L-type calcium channel antagonists and (±)-Bay K8644 on nerve-induced catecholamine secretion from bovine perfused adrenal glands. *Br J Pharmacol* 121: 381–388, 1997.
29. **Pruneau D and Belichard P.** Haemodynamic and humoral effects of ω-conotoxin GVIA in normotensive and spontaneously hypertensive rats. *Eur J Pharmacol* 211: 329–335, 1992.
30. **Randall A and Tsien RW.** Pharmacological dissection of multiple types of Ca^{2+} channel currents in rat cerebellar granule neurons. *J Neurosci* 15: 2995–3012, 1995.
31. **Santana F, Michelena P, Jaén R, García AG, and Borges R.** Calcium channel subtypes and exocytosis in chromaffin cells: a different view from the intact rat adrenal. *Naunyn Schmiedebergs Arch Pharmacol* 360: 33–37, 1999.
32. **Serone AP and Angus JA.** Role of N-type calcium channels in autonomic neurotransmission in guinea-pig isolated left atria. *Br J Pharmacol* 127: 927–934, 1999.
33. **Smith AB and Cunnane TC.** Multiple calcium channels control neurotransmitter release from rat postganglionic sympathetic nerve terminals. *J Physiol* 499: 341–349, 1997.
34. **Wakade AR.** Studies on secretion of catecholamines evoked by acetylcholine or transmural electrical stimulation of the rat adrenal gland. *J Physiol* 313: 463–480, 1981.
35. **Winer BJ.** *Statistical Principles in Experimental Design* (2nd ed.). New York: McGraw-Hill, 1971.
36. **Wright CE and Angus JA.** Prolonged cardiovascular effects of the N-type Ca^{2+} channel antagonist omega-conotoxin GVIA in conscious rabbits. *J Cardiovasc Pharmacol* 30: 392–399, 1997.
37. **Yahagi N, Akiyama T, and Yamazaki T.** Effects of ω-conotoxin GVIA on cardiac sympathetic nerve function. *J Auton Nerv Syst* 68: 43–48, 1998.

Available online at www.sciencedirect.com
SCIENCE DIRECT®
ELSEVIER
Journal of Electron Spectroscopy and Related Phenomena 137–140 (2004) 699–704
JOURNAL OF ELECTRON SPECTROSCOPY and Related Phenomena
www.elsevier.com/locate/elspec

Portable X-ray generator utilizing a cerium-target radiation tube for angiography

E. Sato [a,*], Y. Hayasi [a], R. Germer [b], E. Tanaka [c], H. Mori [d], T. Kawai [e], T. Ichimaru [f], S. Sato [g], K. Takayama [h], H. Ido [i]

[a] *Department of Physics, Iwate Medical University, Morioka 020-0015, Japan*
[b] *ITP, FHTW FB1 and TU-Berlin, D 12249 Berlin, Germany*
[c] *Department of Nutritional Science, Faculty of Applied Bio-science, Tokyo University of Agriculture, Setagayaku 156-8502, Japan*
[d] *Department of Cardiac Physiology, National Cardiovascular Center Research Institute, Osaka 565-8565, Japan*
[e] *Electron Tube Division #2, Hamamatsu Photonics Inc., Iwata-gun 438-0193, Japan*
[f] *Department of Radiological Technology, School of Health Sciences, Hirosaki University, Hirosaki 036-8564, Japan*
[g] *Department of Microbiology, School of Medicine, Iwate Medical University, Morioka 020-8505, Japan*
[h] *Shock Wave Research Center, Institute of Fluid Science, Tohoku University, Sendai 980-8577, Japan*
[i] *Department of Applied Physics and Informatics, Faculty of Engineering, Tohoku Gakuin University, Tagajo 985-8537, Japan*

Available online 15 April 2004

Abstract

The development of a portable X-ray generator with a cerium-target tube and its application to angiography are described. The portable X-ray generator consists of a main controller, a unit with a Cock–Croft circuit and an X-ray tube, and a personal computer. Negative high voltages are applied to the cathode electrode in the X-ray tube, and the tube voltage and current are regulated by the controller or the computer. The X-ray tube is a glass-enclosed double-focus diode with a cerium target and a 0.5 mm-thick beryllium window. The maximum tube voltage and current were 60 kV and 0.8 mA, respectively. The focal-spot sizes were 4 mm × 4 mm (large) and 1 mm × 1 mm (small), respectively. Angiography was performed with a computed radiography system using iodine-based microspheres. The tube voltage, the current, the distance between the imaging plate and the X-ray source, and the spot size were 60 kV, 0.4 mA, 1.5 m, and small, respectively. In this angiography, we observed coronary arteries and fine blood vessels of about 50 μm or less with high contrasts.

Keywords: Cerium-target X-ray tube; Cerium characteristic X-rays; K-absorption edge; High contrast angiography; Microangiogrphy

1. Introduction

In conjunction with single crystals, synchrotrons generate monochromatic X-rays. These rays play an important role in parallel radiography and have been employed to perform high-contrast micro-angiography [1] and phase imaging [2–4]. However, it is difficult to obtain sufficient machine times for various research projects including medical applications.

So far, several different flash X-ray generators have been developed [5,6], and soft generators [7–12] with photon energies of lower than 150 keV can be employed to perform biomedical radiography. In order to produce monochromatic X-rays, plasma flash X-ray generators [13–16] are useful, since quite intense and sharp characteristic X-rays such as lasers have been produced from weakly ionized linear plasmas of nickel, copper and molybdenum, while bremsstrahlung rays are hardly detected at all. Using these generators, the characteristic X-ray intensity substantially increased with corresponding increases in the charging voltage.

Since K-series characteristic X-rays from cerium target are absorbed effectively by iodine-based contrast mediums, a cerium-target X-ray tube is very useful in order to perform high-contrast angiography. On the other hand, cerium is a rare earth element and has a high reactivity, and it is difficult to design the target. However, the development of a cerium-target tube for high-contrast angiography has long been wished for.

* Corresponding author.
E-mail address: dresato@iwate-med.ac.jp (E. Sato).

0368-2048/$ – see front matter © 2004 Elsevier B.V. All rights reserved.
doi:10.1016/j.elspec.2004.02.011

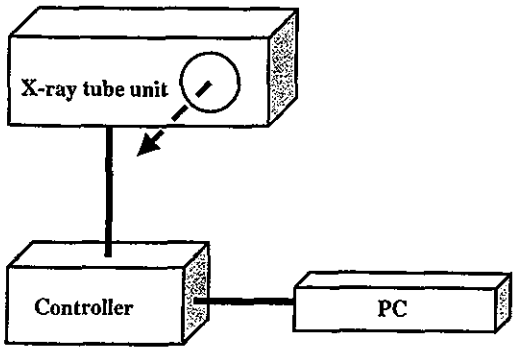

Fig. 1. Block diagram of the portable X-ray generator with a cerium-target radiation tube, which is specially used for angiography using iodine-based contrast mediums. The negative high voltage is applied to the cathode electrode, and the tube current is regulated by the filament temperature. Although the X-ray tube is a double-focus type, we usually employ a small focus in order to measure the radiographic characteristics and to perform angiography.

In the present research, we developed a portable X-ray generator with a cerium-target tube, used to perform preliminary study on angiography achieved with cerium K-series characteristic X-rays.

2. Generator

Fig. 1 shows the block diagram of the X-ray generator, which consists of a main controller, an X-ray tube unit with a Cockcroft circuit and a cerium-target tube, and a personal computer. The negative high-voltage is applied to the cathode electrode, and the anode (target) is connected to the ground potential. In this experiment, the tube voltage was regulated from 40 to 65 kV, and the tube current was regulated within 0.8 mA by the filament temperature. The exposure time is controlled in order to obtain optimum X-ray intensity, and the X-ray tube is a double-focus type with focal-spot dimensions of approximately 4 mm × 4 mm (large spot) and 1 mm × 1 mm (small spot), respectively. The maximum tube current is determined by the spot dimensions, and the currents of small and large spots are 0.4 and 0.8 mA, respectively.

3. Characteristics

3.1. X-ray intensity

X-ray intensity was measured by a Victoreen 660 ionization chamber at 1.0 m from the X-ray source using a small spot with an exposure time of 1.0 s (Fig. 2). At a constant tube current of 40 μA, the X-ray intensity increased when the tube voltage was increased. The intensity was roughly in proportion to the tube current at a constant tube voltage of 60 kV. In this measurement, the intensity with a tube voltage of 60 kV and a current of 90 μA was 2.14 μC/kg at 1.0 m from the source with errors of less than 0.2%.

3.2. X-ray source

In order to measure images of the X-ray source, we employed a pinhole camera with a hole diameter of 50 μm in conjunction with a computed radiography (CR) system (Fig. 3) [17]. When the tube voltage was increased, the spot intensity increased slightly, and spot dimensions seldom varied and had values of approximately 1 mm × 1 mm.

3.3. X-ray spectra

In order to measure X-ray spectra, we employed a cadmium tellurium detector (CDTE2020X, Hamamatsu Photonics Inc.) (Fig. 4). Compared with a germanium detector, this detector has lower energy resolutions. When the tube voltage was increased, both the characteristic X-ray intensity and the maximum photon energy of bremsstrahlung X-rays increased. According to insertion of a monochromatic cerium oxide filter, quasi-monochromatic X-rays were obtained.

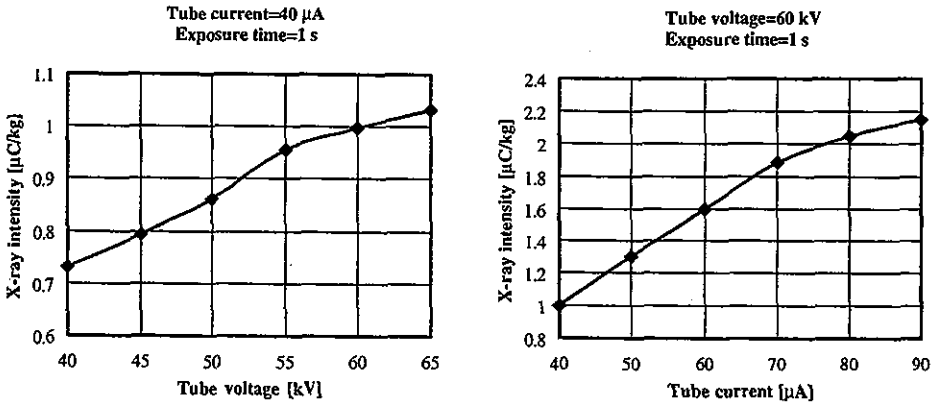

Fig. 2. X-ray intensity measured at 1.0 m from the X-ray source according to changes in the tube voltage and current. In the measurement, we employed an ionization chamber without using a monochromatic filter.

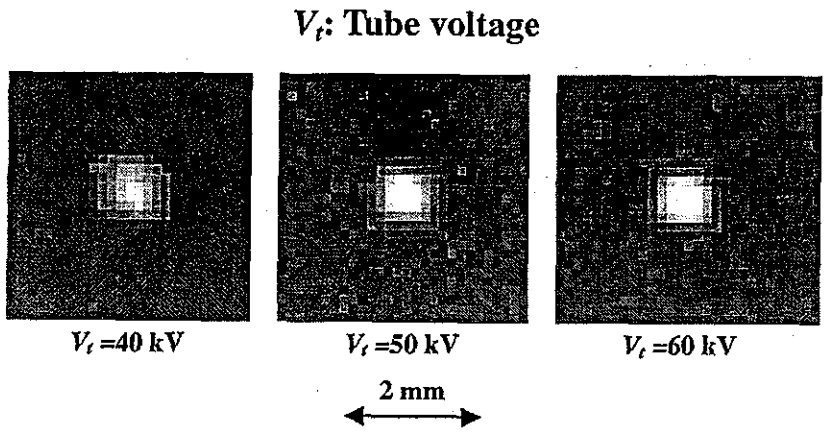

Fig. 3. Images of the X-ray source measured by a 100 mm diameter pinhole with changes in the tube voltage.

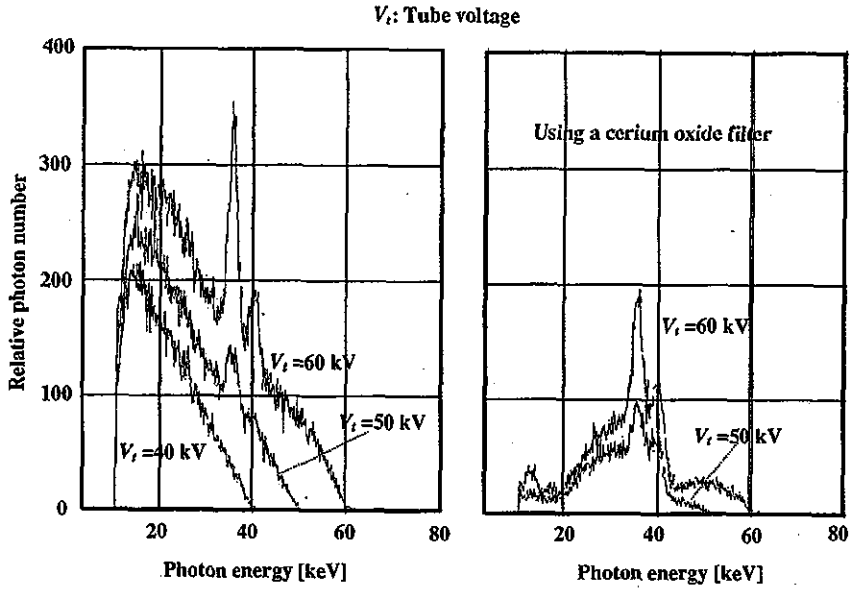

Fig. 4. X-ray spectra measured by a cadmium tellurium detector with changes in the tube voltage.

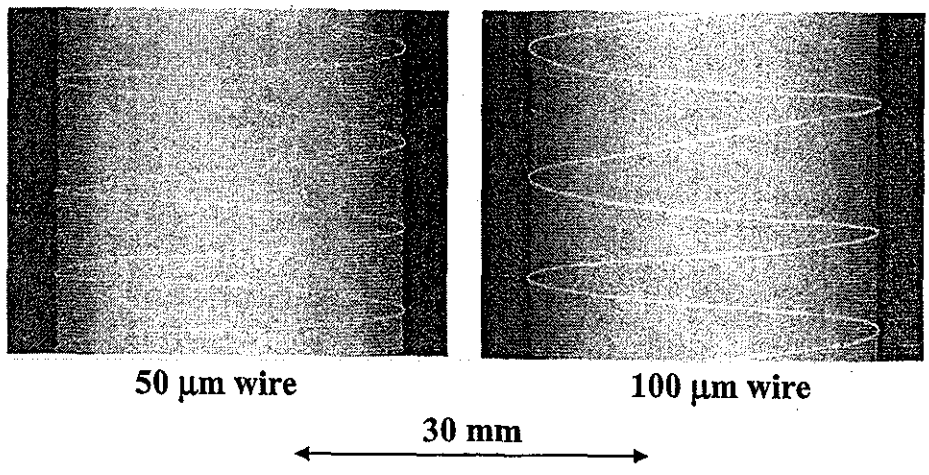

Fig. 5. Radiograms of tungsten wires around a rod made of PMMA used for estimating the image resolution.

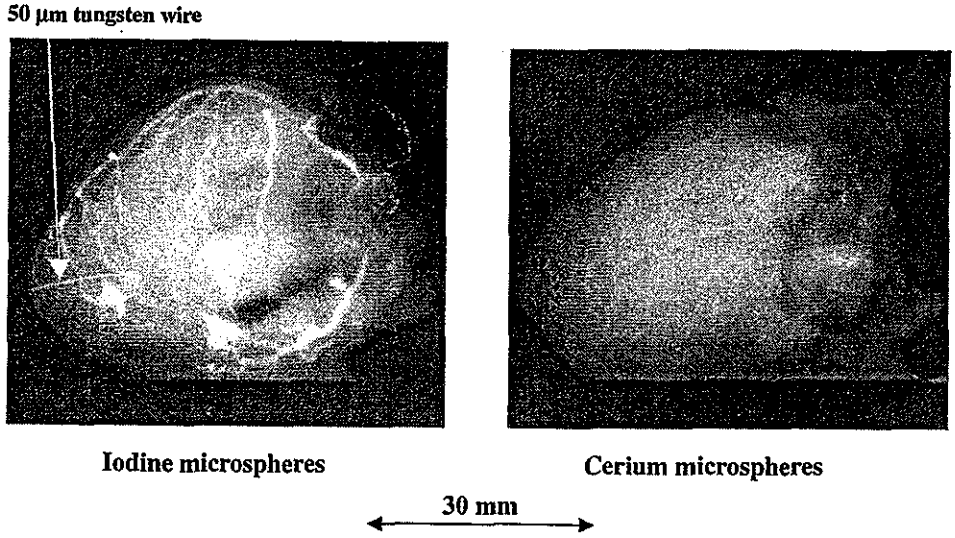

Fig. 6. Angiograms of rabbit hearts using (a) iodine and (b) cerium microspheres.

4. Angiography

The angiography was performed by a CR system (Konica Regius 150) using the monochromatic filter, and the distance (between the X-ray source and the imaging plate) and the tube voltage were 1.5 m and 60 kV, respectively.

Firstly, rough measurements of image resolution were made using wires. Fig. 5 shows radiograms of tungsten wires coiled around rods made of polymethyl methacrylate (PMMA). Although the image contrast increased with increases in the wire diameter, a 50 μm diameter wire could be observed.

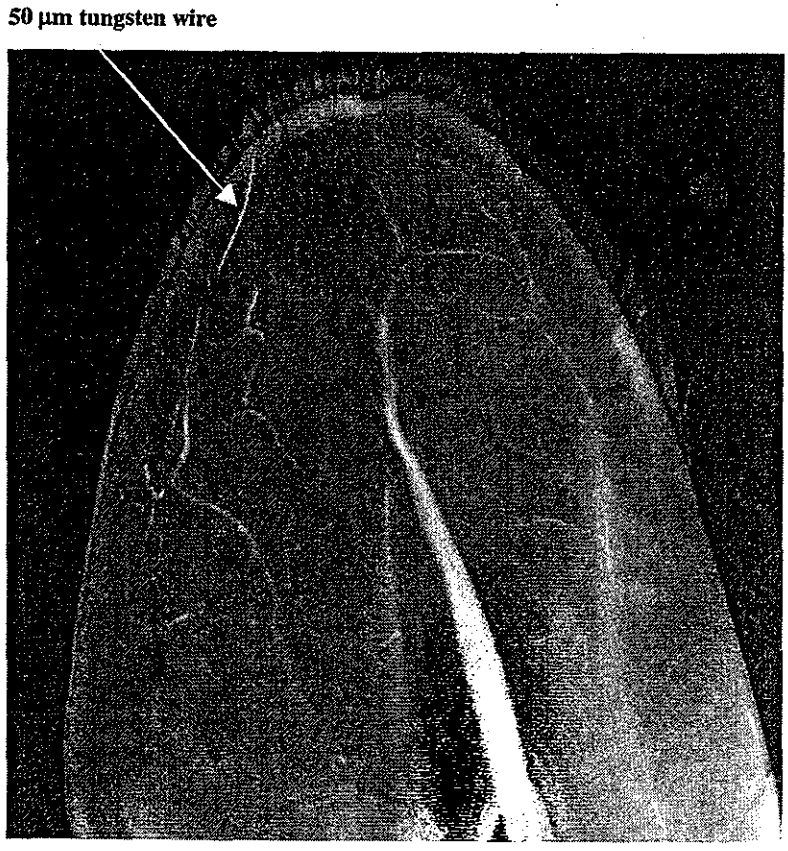

Fig. 7. Angiograms of the external ear of a rabbit using iodine-based microspheres. In this angiography, we employed a 50 μm tungsten wire to roughly determine the diameters of blood vessels.

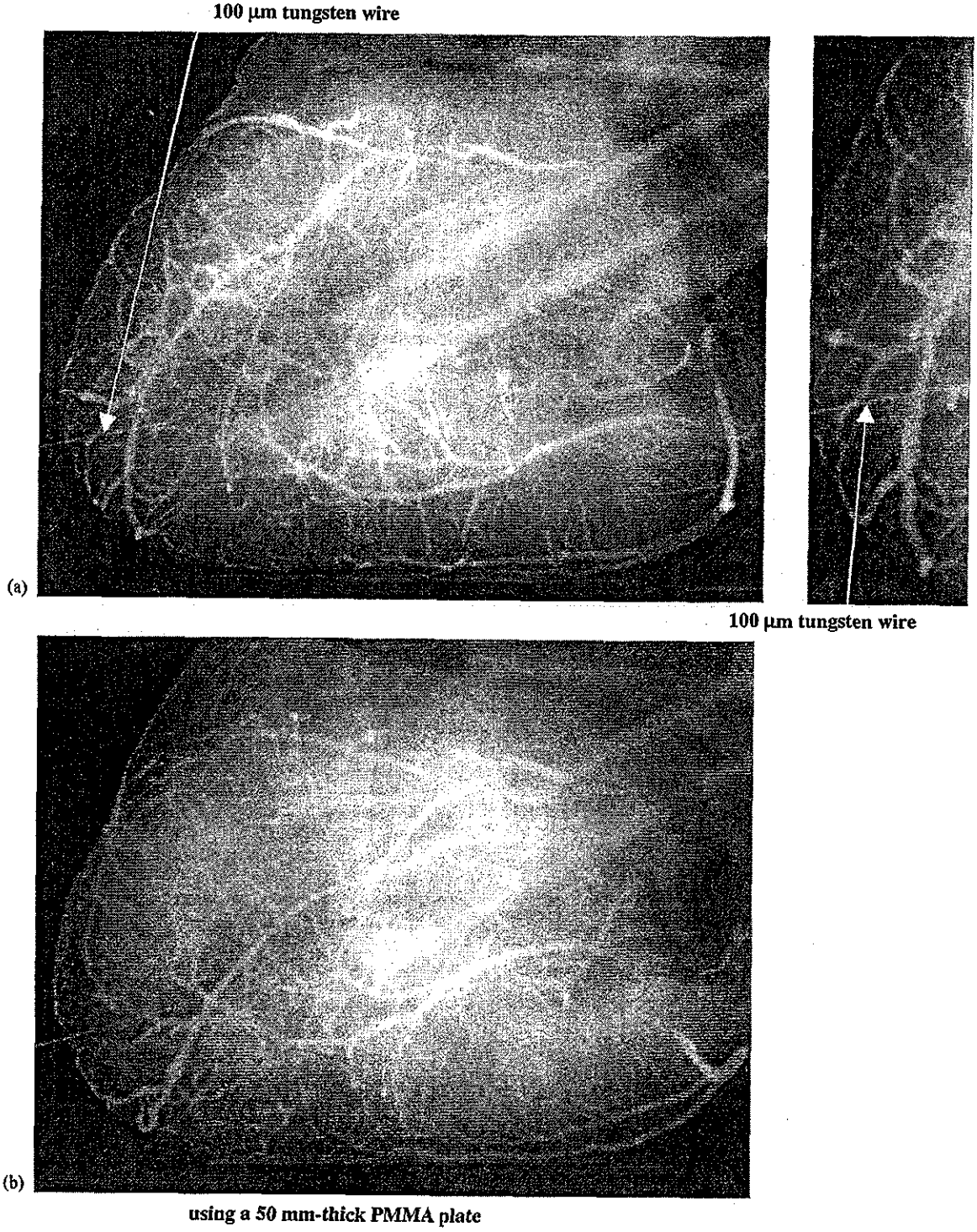

Fig. 8. Angiograms of an extracted heart of a dog. (a) Normal image and (b) image using a 50 mm PMMA plate set in front of the heart, facing the X-ray source.

Angiograms of rabbit hearts are shown in Fig. 6. These two images were obtained using iodine and cerium microspheres of 15 μm in diameter. In case where the cerium spheres were employed, the coronary arteries were barely visible. Fig. 7 shows an angiogram of the external ear of a rabbit using iodine spheres, and fine blood vessels of about 50 μm are clearly visible. In angiography of a larger heart extracted from a dog, using iodine spheres, a 50 mm thick PMMA plate was set in front of the heart facing X-ray source, and image contrast of coronary arteries decreased slightly with increases in the plate thickness (Fig. 8).

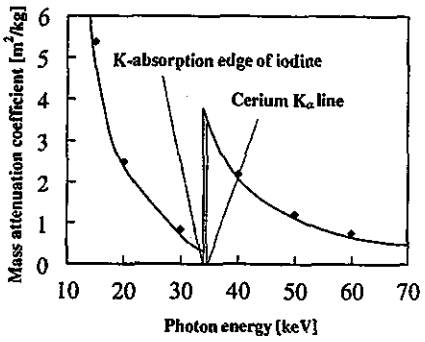

Fig. 9. Relation between the mass absorption coefficient of iodine and the photon energy of cerium Kα line.

5. Discussion

Cerium is a rare earth element and has a high reactivity. However, the average photon energy of Kα lines is 34.566 keV, and iodine spheres with a K-absorption edge of 33.155 keV absorb the lines easily (Fig. 9). Next, since the spheres easily transmit bremsstrahlung X-rays with energies of lower than the edge, it is important that the rays be absorbed as much as possible before angiography in order to increase the image contrast.

In rough measurement of image resolution, we obtained resolutions of 50 μm or less, and high-contrast blood vessels could be observed using a CR system. Although neogenetic fine blood vessels in recovery can be observed, the image resolution of the CR system should be improved as much as possible, and a dynamic CR system such as a flat panel system is useful to observe blood flows.

In this research, we developed a low-dose-rate X-ray tube in order to perform preliminary study on angiography using iodine-based contrast mediums. Because we are designing a high-dose-rate tube to decrease the exposure time, the K-series characteristic X-rays from cerium target can be employed to perform angiography for cases of cardiovascular disease.

6. Summary

In summary, we developed, new portable X-ray generator with a cerium-target tube and succeeded in producing K-series characteristic X-rays of cerium, which can be absorbed easily by iodine-based contrast mediums. Both the characteristic and bremsstrahlung X-ray intensities increased with corresponding increases in the tube voltage, and quasi-monochromatic X-rays were produced by a cerium oxide filter. In this preliminary experiment, although the maximum tube voltage and current were 65 kV and 0.4 mA, respectively, the voltage and current could be increased. Subsequently, we observed a 50 μm tungsten wire easily, and high-contrast angiography was performed using a CR system with an imaging plate.

Acknowledgements

This work was supported by Grants-in-Aid for Scientific Research and Advanced Medical Scientific Research from MECSST (12670902, 13470154, and 13877114), Grants from Keiryo Research Foundation, JST (Test of Fostering Potential), NEDO, and MHLW (HLSRG, RAMT-nano-001, RHGTEFB-genome-005, and RGCD13C-1).

References

[1] H. Mori, K. Hyodo, E. Tanaka, M.U. Mohammed, A. Yamakawa, Y. Shinozaki, H. Nakazawa, Y. Tanaka, T. Sekka, Y. Iwata, S. Honda, K. Umetani, H. Ueki, T. Yokoyama, K. Tanioka, M. Kubota, H. Hosaka, N. Ishizawa, M. Ando, Radiology 201 (1996) 173.
[2] T.J. Davis, D. Gao, T.E. Gureyev, A.W. Stevenson, S.W. Wilkims, Nature 373 (1995) 595.
[3] A. Momose, T. Takeda, Y. Itai, K. Hirano, Nature Med. 2 (4) (1996) 473.
[4] A. Ishisaka, H. Ohara, C. Honda, Opt. Rev. 7 (2000) 566.
[5] A. Mattsson, Phys. Scripta 5 (1972) 99.
[6] R. Germer, J. Phys. E Sci. Instrum. 12 (1979) 336.
[7] E. Sato, S. Kimura, S. Kawasaki, H. Isobe, K. Takahashi, Y. Tamakawa, T. Yanagisawa, Rev. Sci. Instrum. 61 (1990) 2343.
[8] E. Sato, M. Sagae, K. Takahashi, A. Shikoda, T. Oizumi, H. Ojima, K. Takayama, Y. Tamakawa, T. Yanagisawa, A. Fujiwara, K. Mitoya, SPIE 2513 (1994) 723.
[9] A. Shikoda, E. Sato, M. Sagae, T. Oizumi, Y. Tamakawa, T. Yanagisawa, Rev. Sci. Instrum. 65 (1994) 850.
[10] E. Sato, K. Takahashi, M. Sagae, S. Kimura, T. Oizumi, Y. Hayasi, Y. Tamakawa, T. Yanagisawa, Med. Biol. Eng. Comput. 32 (1994) 289.
[11] K. Takahashi, E. Sato, M. Sagae, T. Oizumi, Y. Tamakawa, T. Yanagisawa, Jpn. J. Appl. Phys. 33 (1994) 4146.
[12] E. Sato, M. Sagae, A. Shikoda, K. Takahashi, T. Oizumi, M. Yamamoto, A. Takabe, K. Sakamaki, Y. Hayasi, H. Ojima, K. Takayama, Y. Tamakawa, SPIE 2869 (1996) 937.
[13] E. Sato, Y. Hayasi, E. Tanaka, H. Mori, T. Kawai, T. Usuki, K. Sato, H. Obara, T. Ichimaru, K. Takayama, H. Ido, Y. Tamakawa, SPIE 4682 (2002) 538.
[14] E. Sato, R. Germer, Y. Hayasi, E. Tanaka, H. Mori, T. Kawai, T. Usuki, K. Sato, H. Obara, M. Zuguchi, T. Ichimaru, H. Ojima, K. Takayama, H. Ido, SPIE 4948 (2002) 604.
[15] E. Sato, Y. Hayasi, R. Germer, E. Tanaka, H. Mori, T. Kawai, H. Obara, T. Ichimaru, K. Takayama, H. Ido, Jpn. J. Med. Imag. Inform. Sci. 20 (2003) 148.
[16] E. Sato, Y. Hayasi, R. Germer, E. Tanaka, H. Mori, T. Kawai, H. Obara, T. Ichimaru, K. Takayama, H. Ido, Jpn. J. Med. Phys. 20 (2003) 123.
[17] E. Sato, K. Sato, Y. Tamakawa, Ann. Rep. Iwate Med. Univ. Sch. Lib. Arts Sci. 35 (2000) 13.

Available online at www.sciencedirect.com
SCIENCE DIRECT
ELSEVIER
Journal of Electron Spectroscopy and Related Phenomena 137–140 (2004) 705–711
JOURNAL OF ELECTRON SPECTROSCOPY and Related Phenomena
www.elsevier.com/locate/elspec

Quasi-monochromatic parallel radiography utilizing a computed radiography system

E. Sato [a,*], Y. Hayasi [a], R. Germer [b], E. Tanaka [c], H. Mori [d], T. Kawai [e], T. Ichimaru [f], S. Sato [g], K. Takayama [h], H. Ido [i]

[a] *Department of Physics, Iwate Medical University, Morioka 020-0015, Japan*
[b] *ITP, FHTW FB1 and TU-Berlin, D 12249 Berlin, Germany*
[c] *Department of Nutritional Science, Faculty of Applied Bio-science, Tokyo University of Agriculture, Setagayaku 156-8502, Japan*
[d] *Department of Cardiac Physiology, National Cardiovascular Center Research Institute, Osaka 565-8565, Japan*
[e] *Electron Tube Division #2, Hamamatsu Photonics Inc., Iwata-gun 438-0193, Japan*
[f] *Department of Radiological Technology, School of Health Sciences, Hirosaki University, Hirosaki 036-8564, Japan*
[g] *Department of Microbiology, School of Medicine, Iwate Medical University, Morioka 020-8505, Japan*
[h] *Shock Wave Research Center, Institute of Fluid Science, Tohoku University, Sendai 980-8577, Japan*
[i] *Department of Applied Physics and Informatics, Faculty of Engineering, Tohoku Gakuin University, Tagajo 985-8537, Japan*

Available online 21 March 2004

Abstract

A fundamental study on quasi-monochromatic parallel radiography using a polycapillary plate and a copper-target X-ray tube is described. The X-ray generator consists of a negative high-voltage power supply, a filament (hot cathode) power supply, and an X-ray tube. The negative high-voltage is applied to the cathode electrode, and the anode electrode is connected to the ground. In this experiment, the tube voltage was regulated from12–25 kV, and the tube current was regulated within 3.0 mA by the filament temperature. The exposure time was controlled in order to obtain optimum X-ray intensity, and the maximum focal spot dimensions were approximately 2 mm × 1.5 mm. The polycapillary plate was J5022-21 (Hamamatsu Photonics Inc.), and the plate thickness was 1.0 mm. The outer, effective, and hole diameters were 87 mm, 77 mm, and 25 μm, respectively. Quasi-monochromatic X-rays were produced using a 10 μm-thick copper filter, and these rays were formed into parallel beams by the polycapillary, and the radiogram was taken using a computed radiography system utilizing imaging plates. In the measurement of image resolution, the resolution fell according to increases in the distance between the chart and imaging plate using a polycapillary. We could observe a 50 μm tungsten wire clearly, and fine blood vessels of approximately 100 μm were visible in angiography.

Keywords: Parallel radiography; Quasi-monochromatic X-ray; Characteristic X-ray; X-ray lens; Polycapillary plate

1. Introduction

Thus far, we have developed several different soft flash X-ray generators [1–8] in order to perform soft radiographies with biomedical applications. In particular, plasma flash X-ray generators [9–11] are very useful to produce fairly high-dose-rate monochromatic X-rays as compared with a synchrotron. When a weakly ionized linear plasma formed using a rod target evaporation, irradiation of quite intense and sharp characteristic X-rays from the plasma axial direction was confirmed.

Monochromatic parallel radiography using synchrotrons plays important roles in microangiography [12] and X-ray phase imaging, [13–15] and further applications have long been wished for. In view of this situation, several different X-ray lenses have been developed [16,17], and a polycapillary plate [18–20] has been shown to be useful to realize a low-priced X-ray system and to perform parallel radiography. Therefore, we performed parallel radiography using a tungsten-target X-ray tube [19] and an X-ray film, and an image resolution of approximately 50 μm or less was obtained.

The tungsten target produced L-series characteristic and bremsstrahlung X-rays with tube voltages of 20–30 kV, and these rays were formed into parallel beams to perform radiography. Thereafter, K-series characteristic X-rays could

* Corresponding author.
E-mail address: dresato@iwate-med.ac.jp (E. Sato).

0368-2048/$ – see front matter © 2004 Elsevier B.V. All rights reserved.
doi:10.1016/j.elspec.2004.02.008

be employed for quasi-monochromatic and monochromatic radiographies using filters. In these cases, the photon energies of characteristic X-rays were determined by the target element.

In this research, we performed preliminary study on quasi-monochromatic parallel radiography utilizing a polycapillary plate, a Computed Radiography (CR) system [21], and a copper-target radiation tube in order to create a new X-ray system to be used instead of the synchrotron.

2. Experimental set-up

Fig. 1 shows the circuit diagram of the X-ray generator, which consists of a negative high-voltage power supply, a filament (hot cathode) power supply, and a copper-target X-ray tube. The negative high-voltage is applied to the cathode electrode, and the anode (target) is connected to the ground. In this experiment, the tube voltage was regulated from 15–25 kV, and the tube current was regulated by the filament temperature and ranged from 1.0–3.0 mA. The exposure time was controlled in order to obtain optimum X-ray intensity.

The experimental set-up for performing parallel radiography is shown in Fig. 2. Quasi-monochromatic X-rays are produced using a 10 μm-thick copper filter, and these rays are formed into parallel beams by a polycapillary plate. The polycapillary is J5022-21 (Hamamatsu Photonics Inc.), and the thickness and the hole diameter of the polycapillary are

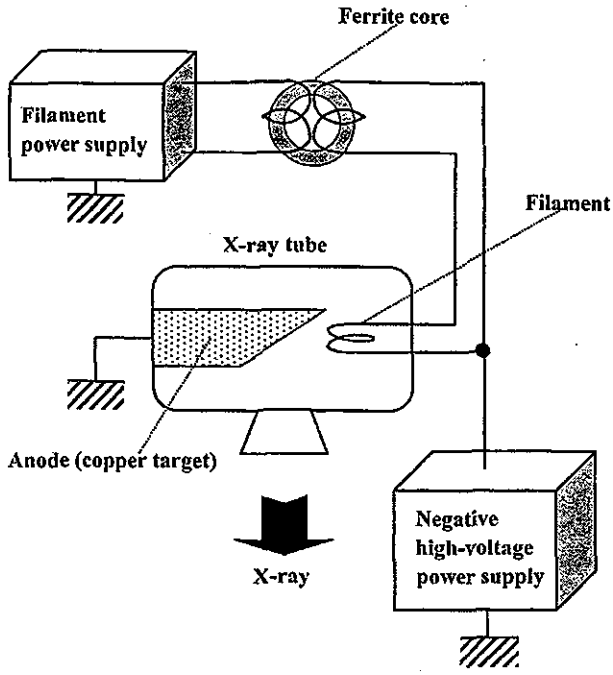

Fig. 1. Circuit diagram of the X-ray generator. Because the negative high voltage is applied to the cathode electrode, the tube voltage is −1 times the cathode voltage. The X-ray tube employs a 0.5 mm-thick beryllium window in order to produce soft X-rays effectively.

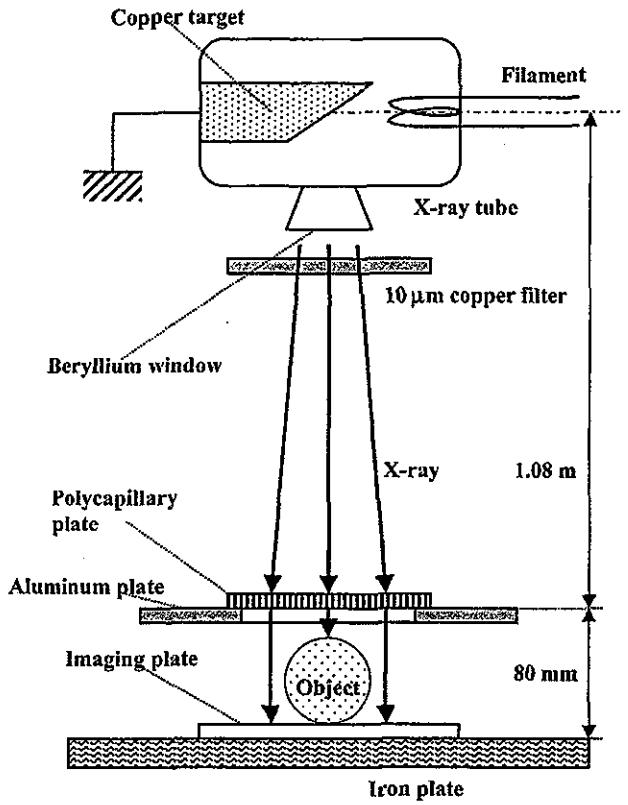

Fig. 2. Experimental set-up for parallel radiography utilizing a polycapillary plate and a CR system. Quasi-monochromatic X-rays are formed into parallel beam by a polycapillary, and the image is taken by a CR system.

1.0 mm and 25 μm, respectively (Fig. 3). Radiography was performed by a CR system (Konica Regius 150) utilizing imaging plates.

The distance between the X-ray source and the polycapillary was 1.08 m, and the polycapillary plate was placed on the aluminum plate, and the distance between the aluminum and imaging plates was regulated by the height of polymethyl methacrylate (PMMA) spacers of 30 mm in height.

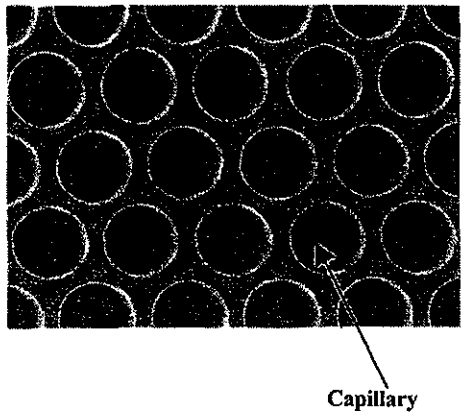

Fig. 3. Magnification of a polycapillary plate with a thickness of 1.0 mm and a hole diameter of 25 μm, respectively.

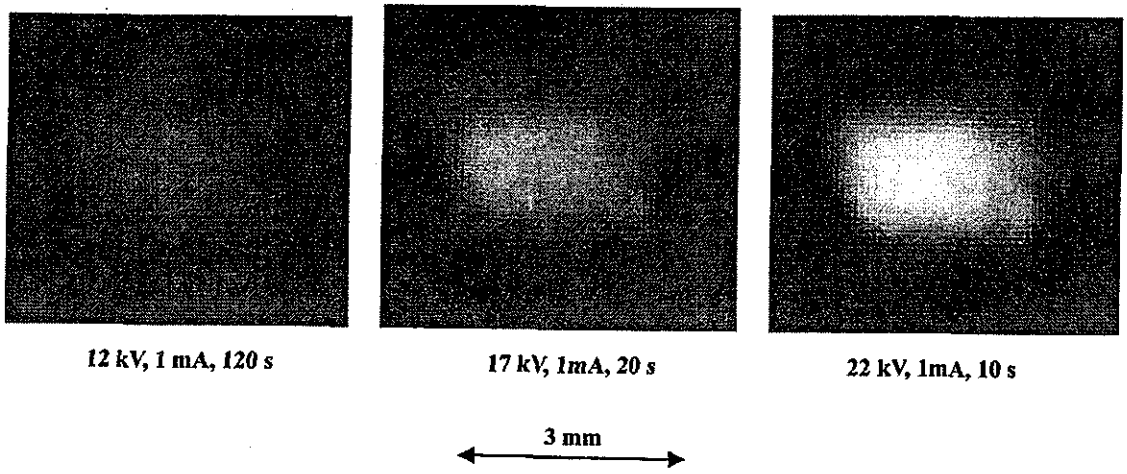

Fig. 4. Images of the X-ray source measured by a 50 μm-diameter pinhole with changes in the tube voltage.

3. Characteristics

3.1. Focal spot

In order to measure images of the X-ray source, we employed a pinhole camera with a hole diameter of 50 μm (Fig. 4). When the tube voltage was increased, the spot intensity increased, and spot dimensions increased slightly and had values of approximately 2 mm × 1.5 mm.

3.2. X-ray spectra

X-ray spectra from the copper-target tube were measured by a transmission-type spectrometer (Fig. 5) with a lithium fluoride curved crystal 0.5 mm in thickness. The spectra were taken by the CR system with a wide dynamic range, and relative X-ray intensity was calculated from Dicom digital data. Fig. 6 shows measured spectra from the copper target. When the tube voltage was increased, the bremsstrahlung X-ray intensity increased, and the characteristic X-ray intensity of K_α and K_β lines also increased. Following insertion of the copper filter, since the bremsstrahlung X-rays with energies higher than the K-absorption edge were absorbed effectively, we observed the edge.

4. Radiography

The quasi-monochromatic radiography was performed with a tube voltage of 20 kV using the filter. Fig. 7 shows radiography for imaging a polycapillary plate, and the radiograms of the polycapillary are shown in Fig. 8. The center of the black spot in the polycapillary radiogram was mainly imaged by direct transmission beams through capillary holes. As shown in this figure, both the spot density and the dimensions hardly varied according to decreases in the polymethyl methacrylate (PMMA) spacer height.

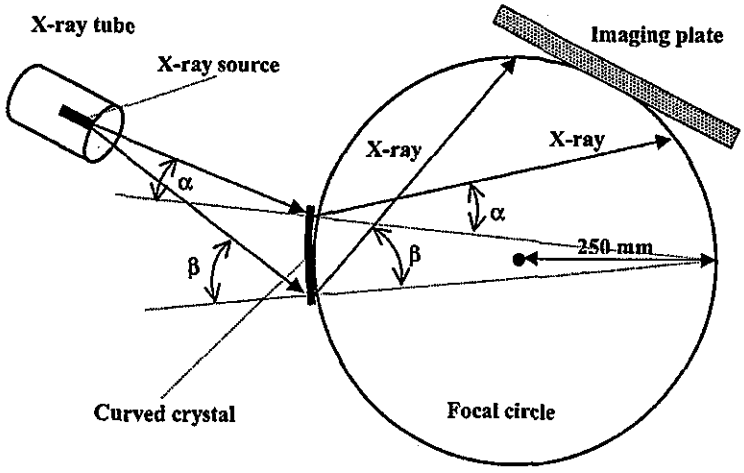

Fig. 5. Transmission-type spectrometer with a lithium fluoride curved crystal and an imaging plate. The X-rays from the source are diffracted by the crystal and are imaged on the imaging plate.

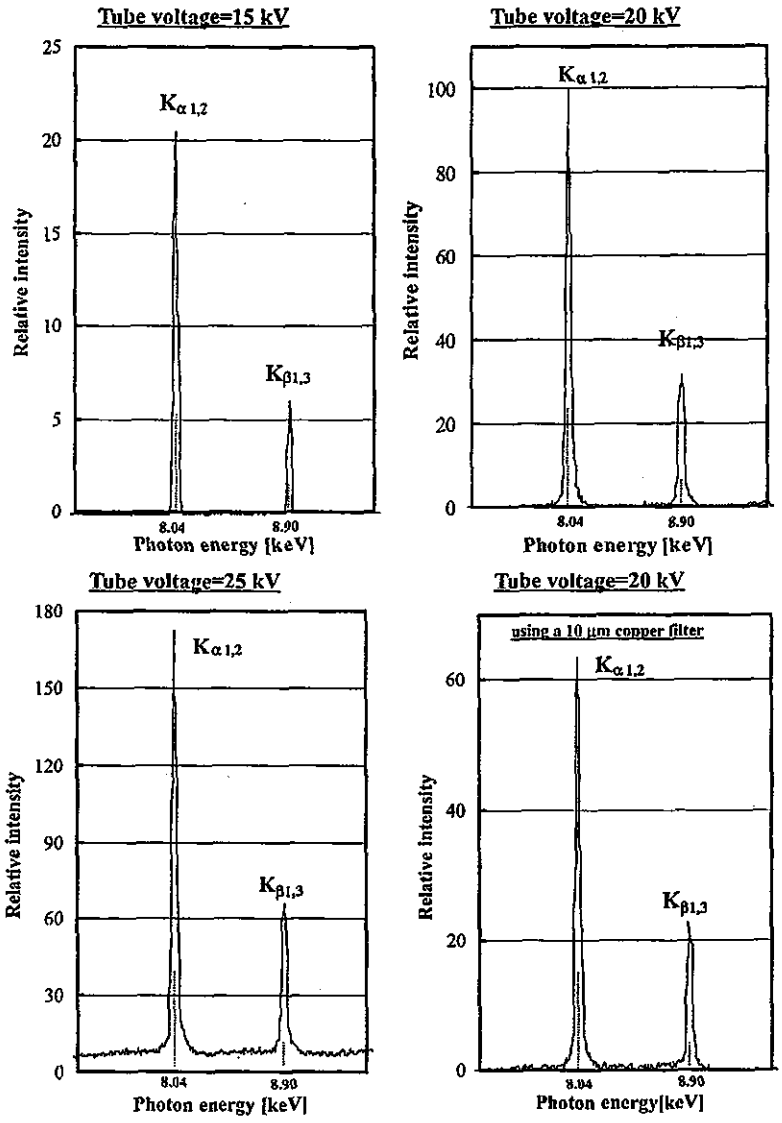

Fig. 6. Measured X-ray spectra according to changes in the tube voltage. Both the bremsstrahlung and characteristic X-ray intensities increased with corresponding increases in the tube voltage, and we determined the conditions for radiography as follows: a tube voltage of 20 kV and a filter thickness of 10 μm.

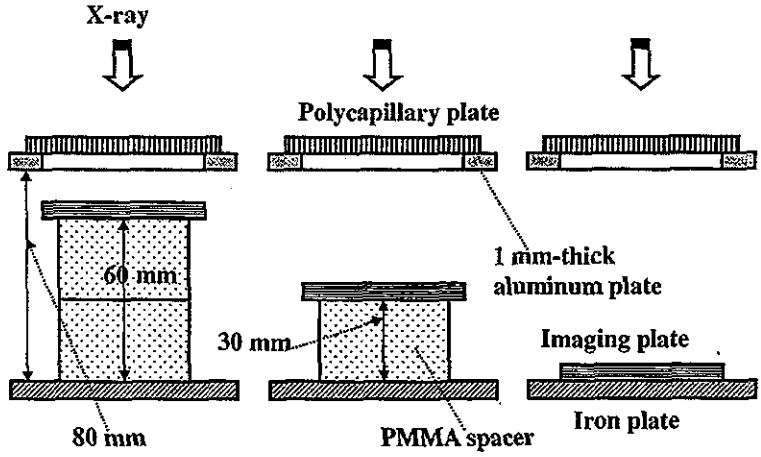

Fig. 7. Radiography for imaging a polycapillary plate according to changes in the distance between the polycapillary and imaging plates. Because the distance was regulated by the spacer thickness, the distance decreased according to increases in the spacer height.

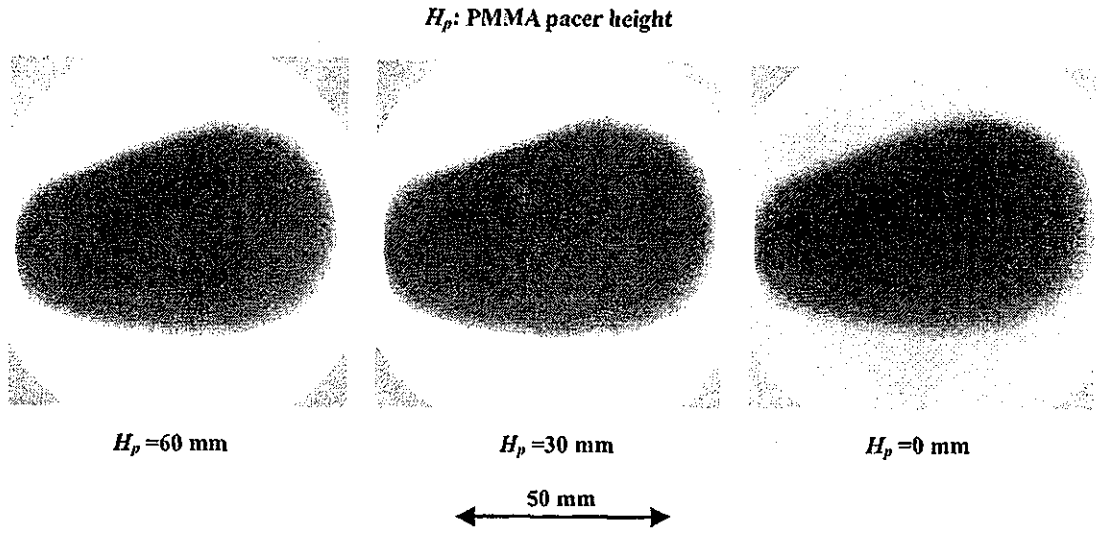

Fig. 8. Radiograms of a polycapillary plate according to changes in the PMMA height.

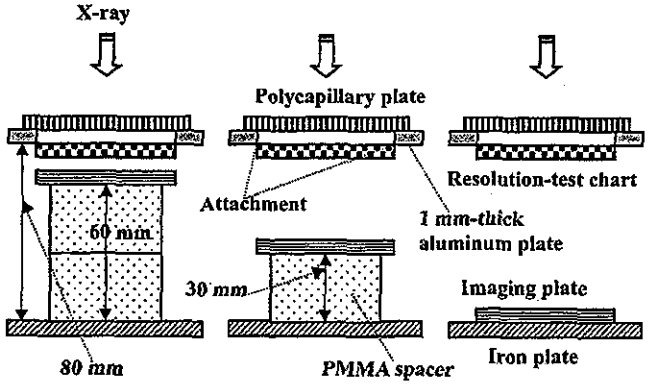

Fig. 9. Radiography for imaging a test chart using a polycapillary plate.

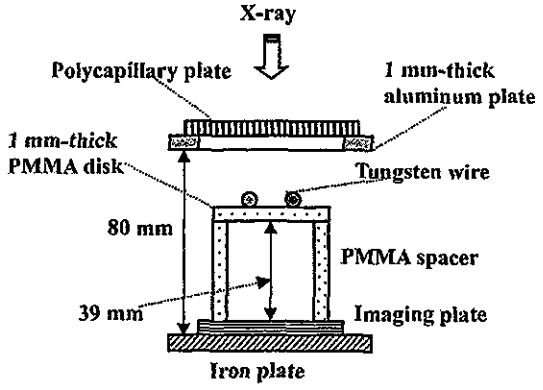

Fig. 11. Radiography for imaging tungsten wires using the polycapillary.

Fig. 9 shows the parallel radiography for imaging a test chart, and the polycapillary was placed on the aluminum plate. In this radiography, when the spacer height was increased, we observed 100 μm lines, and the image dimensions decreased slightly (Fig. 10).

Figs. 11 and 12 show radiography and the radiogram of tungsten wires on a PMMA spacer, respectively. Although the image contrast increased with increases in the wire diameter, a 50 μm-diameter wire could be observed. An angiography of a rabbit heart is shown in Fig. 13; iodine-based

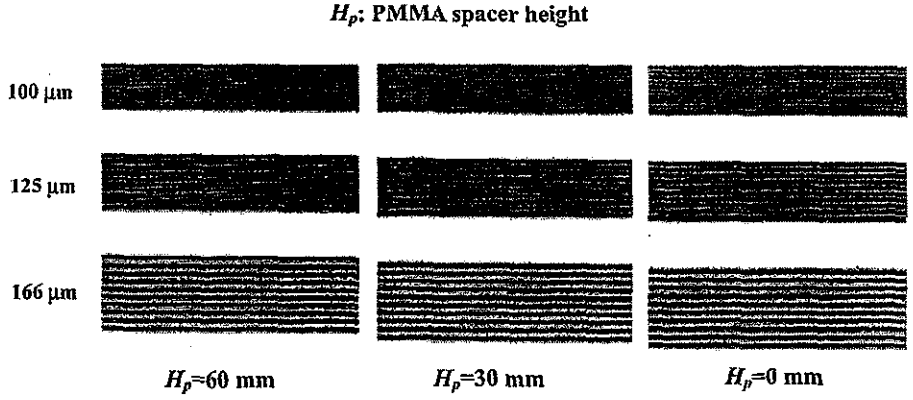

Fig. 10. Radiograms of a test chart using the polycapillary according to changes in the height.

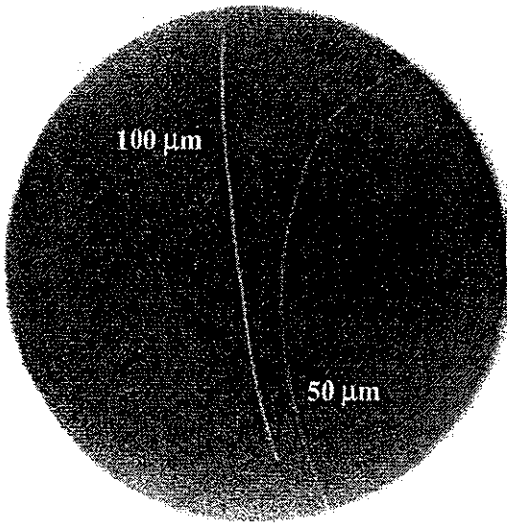

Fig. 12. Radiograms of tungsten wires on a PMMA spacer.

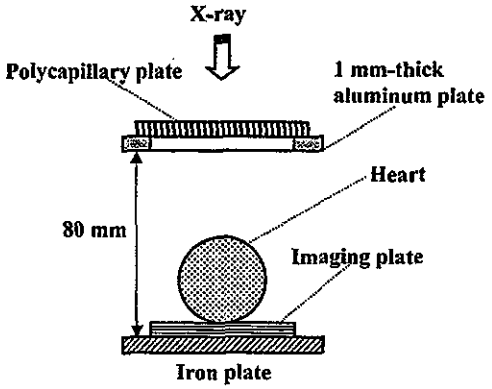

Fig. 13. Parallel angiography of a heart extracted from a rabbit using iodine-based microspheres.

microspheres of 15 μm-diameter were used, and fine blood vessels of about 100 μm were clearly visible (Fig. 14).

5. Discussion

Using this polycapillary plate, we performed a quasi-monochromatic parallel radiography system using a polycapillary plate in conjunction with a CR system.

If we assume that the incident angle for reflection in the capillary hole is constant, the X-ray intensity without absorbing I_0, the transmission intensity I_t, the reflecting intensity I_r, and the intensity for parallel radiography I may be given by (Fig. 15):

$$I_0 = K_1 \sum_{i=1}^{n} I_k(E_i) \exp\{-\mu(E_i)a\}, \quad (1)$$

$$I_t \cong K_2 \sum_{i=1}^{n} I_k(E_i) \exp\{-\mu(E_i)a - \mu_c(E_i)b\}, \quad (2)$$

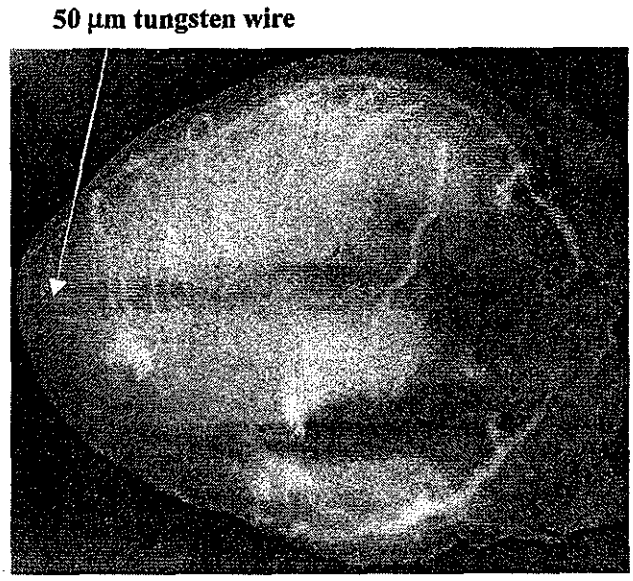

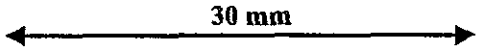

Fig. 14. Angiogram of the heart using the polycapillary.

$$I_r \cong K_3 \sum_{i=1}^{n} I_k(E_i) \exp\{-\mu(E_i)a\} \cdot R(E_i)^m, \quad (3)$$

$$I \cong I_0 + I_r \gg I_t, \quad (4)$$

where $I_k(E_i)$ is the ith characteristic X-ray intensity from the tube, $\mu(E_i)$ the linear absorption coefficient of copper filter, $\mu_c(E_i)$ is the linear absorption coefficient of capillary glass, $R(E_i)$ is the reflecting power ($1 \geqq R(E_i) \geqq 0$), m is the number of reflection, n is the number of characteristic X-rays, a is the filter thickness, b is capillary thickness, and K_1–K_3 are constants.

In this research, we performed parallel radiography achieved with a polycapillary plate in conjunction with quasi-monochromatic X-rays, and higher image resolutions as compared with those obtained without using the plate were obtained. Currently, because the resolution improves

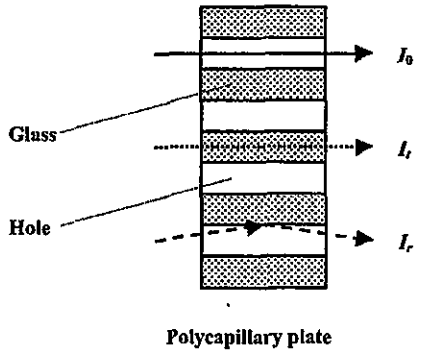

Fig. 15. Characteristic X-ray transmissions in the polycapillary plate. In the parallel radiography, the radiographic object is taken by both the direct transmission rays through capillaries I_0 and the reflection rays on the insides of holes I_r.

with corresponding decreases in the hole diameter of the capillary, this system can be applied to image a wide variety of objects in various fields including medical radiography.

6. Summary

In summary, we developed a conventional quasi-monochromatic parallel radiography system utilizing a polycapillary plate with a hole diameter of 25 μm and a CR system. Quasi-monochromatic characteristic X-rays were obtained by a 10 μm-thick copper filter with a tube voltage of 20 kV. The X-rays from the tube were formed into parallel beams in order to perform radiography. The image dimension increased slightly with corresponding increases in the distance between the radiographic object and the imaging plate, and we observed a 50 μm tungsten wire and fine blood vessels clearly.

Acknowledgements

This work was supported by Grants-in-Aid for Scientific Research and Advanced Medical Scientific Research from MECSST (12670902, 13470154, and 13877114), Grants from Keiryo Research Foundation, JST (Test of Fostering Potential), NEDO, and MHLW (HLSRG, RAMT-nano-001, RHGTEFB-genome-005, and RGCD13C-1).

References

[1] E. Sato, S. Kimura, S. Kawasaki, H. Isobe, K. Takahashi, Y. Tamakawa, T. Yanagisawa, Rev. Sci. Instrum. 61 (1990) 2343.
[2] E. Sato, A. Shikoda, S. Kimura, M. Sagae, T. Oizumi, K. Takahashi, Y. Hayasi, T. Shoji, K. Shishido, Y. Tamakawa, T. Yanagisawa, SPIE 1801 (1992) 628.
[3] E. Sato, M. Sagae, K. Takahashi, T. Oizumi, H. Ojima, K. Takayama, Y. Tamakawa, T. Yanagisawa, A. Fujiwara, K. Mitoya, SPIE 2513 (1994) 649.
[4] E. Sato, M. Sagae, K. Takahashi, A. Shikoda, T. Oizumi, H. Ojima, K. Takayama, Y. Tamakawa, T. Yanagisawa, A. Fujiwara, K. Mitoya, SPIE 2513 (1994) 723.
[5] A. Shikoda, E. Sato, M. Sagae, T. Oizumi, Y. Tamakawa, T. Yanagisawa, Rev. Sci. Instrum. 65 (1994) 850.
[6] E. Sato, K. Takahashi, M. Sagae, S. Kimura, T. Oizumi, Y. Hayasi, Y. Tamakawa, T. Yanagisawa, Med. Biol. Eng. Comput. 32 (1994) 289.
[7] K. Takahashi, E. Sato, M. Sagae, T. Oizumi, Y. Tamakawa, T. Yanagisawa, Jpn. J. Appl. Phys. 33 (1994) 4146.
[8] E. Sato, M. Sagae, A. Shikoda, K. Takahashi, T. Oizumi, M. Yamamoto, A. Takabe, K. Sakamaki, Y. Hayasi, H. Ojima, K. Takayama, Y. Tamakawa, SPIE 2869 (1996) 937.
[9] E. Sato, R. Germer, Y. Hayasi, E. Tanaka, H. Mori, T. Kawai, T. Usuki, K. Sato, H. Obara, M. Zuguchi, T. Ichimaru, H. Ojima, K. Takayama, H. Ido, SPIE 4948 (2002) 604.
[10] E. Sato, Y. Hayasi, R. Germer, E. Tanaka, H. Mori, T. Kawai, H. Obara, T. Ichimaru, K. Takayama, H. Ido, Jpn. J. Med. Imag. Inform. Sci. 20 (2003) 148.
[11] E. Sato, Y. Hayasi, R. Germer, E. Tanaka, H. Mori, T. Kawai, H. Obara, T. Ichimaru, K. Takayama, H. Ido, Jpn. J. Med. Phys. 20 (2003) 123.
[12] H. Mori, K. Hyodo, E. Tanaka, M.U. Mohammed, A. Yamakawa, Y. Shinozaki, H. Nakazawa, Y. Tanaka, T. Sekka, Y. Iwata, S. Honda, K. Umetani, H. Ueki, T. Yokoyama, K. Tanioka, M. Kubota, H. Hosaka, N. Ishizawa, M. Ando, Radiology 201 (1996) 173.
[13] T.J. Davis, D. Gao, T.E. Gureyev, A.W. Stevenson, S.W. Wilkims, Nature 373 (1995) 595.
[14] A. Momose, T. Takeda, Y. Itai, K. Hirano, Nat. Med. 2 (4) (1996) 473.
[15] A. Ishisaka, H. Ohara, C. Honda, Opt. Rev. 7 (2000) 566.
[16] A.A. Bzhanmikov, N. Langhoff, J. Schmalz, R. Wedell, V.L. Beloglazov, N.F. Lebedev, SPIE 3444 (1998) 430.
[17] Q.F. Xiao, S.V. Poturaef, Nucl. Instr. Meth. Phys. Res. A 347 (1994) 376.
[18] E. Sato, Y. Hayasi, E. Tanaka, H. Mori, T. Kawai, H. Obara, T. Ichimaru, K. Takayama, H. Ido, T. Usuki, K. Sato, Y. Tamakawa, SPIE 4508 (2001) 176.
[19] E. Sato, H. Toriyabe, Y. Hayasi, E. Tanaka, H. Mori, T. Kawai, T. Usuki, K. Sato, H. Obara, T. Ichimaru, K. Takayama, H. Ido, Y. Tamakawa, SPIE 4682 (2002) 298.
[20] E. Sato, Y. Hayasi, T. Usuki, K. Sato, H. Ojima, K. Takayama, H. Ido, in: Proceedings of the 3rd Korea-Japan Joint Meeting on Medical Physics, Gyeongju, 2002, p. 400.
[21] E. Sato, K. Sato, Y. Tamakawa, Ann. Rep. Iwate Med. Univ. Sch. Lib. Arts Sci. 35 (2000) 13.

Available online at www.sciencedirect.com
SCIENCE DIRECT®
ELSEVIER
Journal of Electron Spectroscopy and Related Phenomena 137–140 (2004) 713–720
JOURNAL OF ELECTRON SPECTROSCOPY and Related Phenomena
www.elsevier.com/locate/elspec

Sharp characteristic X-ray irradiation from weakly ionized linear plasma

E. Sato [a,*], Y. Hayasi [a], R. Germer [b], E. Tanaka [c], H. Mori [d], T. Kawai [e], T. Ichimaru [f], S. Sato [g], K. Takayama [h], H. Ido [i]

[a] *Department of Physics, Iwate Medical University, Morioka 020-0015, Japan*
[b] *ITP, FHTW FB1 and TU-Berlin, D 12249 Berlin, Germany*
[c] *Department of Nutritional Science, Faculty of Applied Bio-science, Tokyo University of Agriculture, Setagayaku 156-8502, Japan*
[d] *Department of Cardiac Physiology, National Cardiovascular Center Research Institute, Osaka 565-8565, Japan*
[e] *Electron Tube Division #2, Hamamatsu Photonics Inc., Iwata-gun 438-0193, Japan*
[f] *Department of Radiological Technology, School of Health Sciences, Hirosaki University, Hirosaki 036-8564, Japan*
[g] *Department of Microbiology, School of Medicine, Iwate Medical University, Morioka 020-8505, Japan*
[h] *Shock Wave Research Center, Institute of Fluid Science, Tohoku University, Sendai 980-8577, Japan*
[i] *Department of Applied Physics and Informatics, Faculty of Engineering, Tohoku Gakuin University, Tagajo 985-8537, Japan*

Available online 21 March 2004

Abstract

In the plasma flash X-ray generator, a high-voltage main condenser of approximately 200 nF is charged up to 50 kV by a power supply, and electric charges in the condenser are discharged to an X-ray tube after triggering the cathode electrode. Flash X-rays are then produced. The X-ray tube is a demountable triode connected to a turbo molecular pump with a pressure of approximately 1 mPa. As electrons from the cathode electrode are roughly focused onto a rod nickel target of 3.0 mm in diameter by the electric field in the X-ray tube, a weakly ionized linear plasma consisting of nickel ions and electrons forms by target evaporation. At a charging voltage of 50 kV, the maximum tube voltage was almost equal to the charging voltage of the main condenser, and the peak current was about 17 kA. When the charging voltage was increased, the linear plasma formed, and the intensities of K-series characteristic X-rays increased. The K-series lines were quite sharp and intense, and hardly any bremsstrahlung rays were detected. The X-ray pulse widths were approximately 700 ns, and the time-integrated X-ray intensity had a value of approximately 30 μC/kg at 1.0 m from the X-ray source at a charging voltage of 50 kV.

Keywords: Flash X-ray; Weakly ionized linear plasma; K-series characteristic X-rays; Quasi-monochromatic X-rays; Monochromatic X-rays

1. Introduction

Flash X-ray generators utilizing condensers are of great technological importance due to their extremely short X-ray durations, and several different types of generators have been developed for specific radiographic applications [1,2]. In particular, flash X-ray generators with energies lower than 150 keV have been developed in order to perform soft radiographies with biomedical applications [3–8], and these generators have large capacity condensers in order to increase the X-ray intensity by increasing electrostatic energy.

Using a gas-discharge capillary [9–12], soft X-ray lasers have been produced to form a linear plasma, in which the laser intensity increases proportionally to the capillary length. However, it is quite difficult to increase the laser photon energy beyond 10 keV. Because there are no X-ray resonators in the high photon energy region, new methods for increasing coherence will be desired in the future.

By forming a weakly ionized linear plasma [13–16] using plate and rod targets, we confirmed the production of intense K-series characteristic X-rays along the plasma axial direction. In these experiments, because we employed a transmission-type X-ray spectrometer utilizing an X-ray film, it was difficult to determine the relative intensities of the characteristic X-rays.

In this paper, we describe a flash X-ray generator utilizing a large capacity condenser of 200 nF and a rod-target

* Corresponding author.
E-mail address: dresato@iwate-med.ac.jp (E. Sato).

0368-2048/$ – see front matter © 2004 Elsevier B.V. All rights reserved.
doi:10.1016/j.elspec.2004.02.009

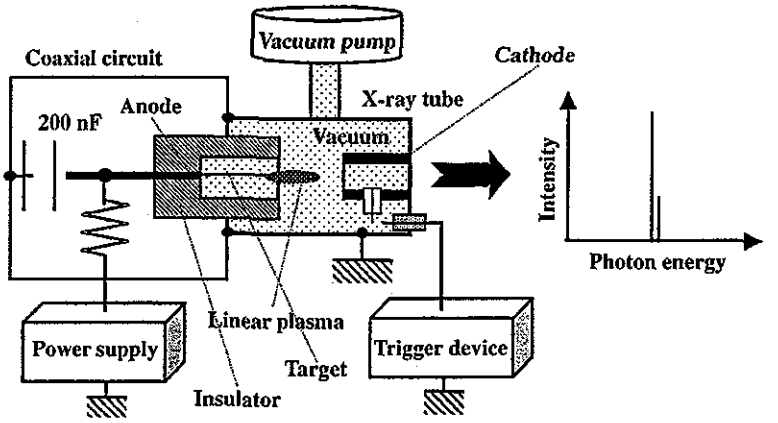

Fig. 1. Block diagram of the high-intensity plasma flash X-ray generator. This generator employs a large capacity condenser in order to increase tl characteristic X-ray intensities in a low photon energy region by increasing the electrostatic energy in the condenser.

radiation tube, used to perform a preliminary experiment for generating intense and sharp monochromatic X-rays by forming a linear nickel plasma cloud around a fine target.

2. Generator

2.1. High-voltage circuit

Fig. 1 shows a block diagram of the high-intensity plasma flash X-ray generator. This generator consists of the following essential components: a high-voltage powe supply, a high-voltage condenser with a capacity of ap proximately 200 nF, a turbo-molecular vacuum pump, krytron pulse generator as a trigger device, and a flas X-ray tube. In this generator, a low-impedance trans mission line is employed in order to increase maximu tube current. The high-voltage main condenser is charge to 50 kV by the power supply, and electric charges i the condenser are discharged to the tube after triggerin the cathode electrode. The plasma flash X-rays are the produced.

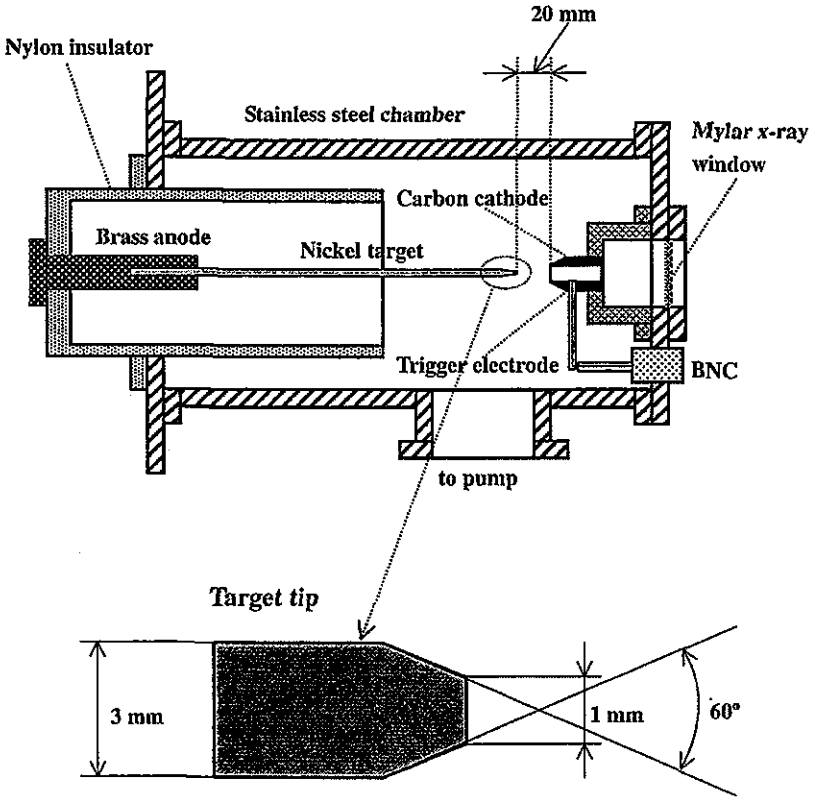

Fig. 2. Schematic drawing of the flash X-ray tube with a rod target. The tube utilizes a long target to form a weakly ionized linear plasma to abso bremsstrahlung X-rays produced in the plasma, which transmits the characteristic X-rays easily due to the absorption coefficient.